Nanoparticles used in dental materials affect cell viability of PC12 cells

Alexandra Isabel Sveinsen Treimo

Thesis submitted for the degree of

Master of Science in Toxicology

60 credits

Department of Biosciences

Faculty of Mathematics and Natural Sciences

UNIVERSITY OF OSLO

June 2018

2018

Nanoparticles used in dental materials affect cell viability of PC12 cells

Alexandra Isabel Sveinsen Treimo

http://www.duo.uio.no

Print: Reprosentralen, Universitetet i Oslo

This project was carried out in collaboration with Nordic Institute of Dental Materials (NIOM).

Acknowledgements

This master's thesis was conducted at the Department of Biosciences at the University of Oslo (UiO) in collaboration with Nordic Institute of Dental Materials (NIOM), Oslo. My supervisors were Kirsten Eline Rakkestad (VKM, NIOM), Katrine Borgå (UiO), Jan Tore Samuelsen (NIOM) and Ragnhild Elisabeth Paulsen (UiO).

Thank you Jon E. Dahl for making this project possible and for the great learning environment and facilities at NIOM. Kirsten and Jan Tore, your knowledge, humor and constructive feedback have made working with you and this master thesis a true joy. I hope we can work together again in the future. A special thank to Else, Bergitte, Solveig and Ida for always helping me. Your support and knowledge have been indispensible. You are a true inspiration to me.

To my friends and family, thank you for all your love, support and for constructive feedback. My love Simon, thank you for always believing in me (and bringing me coffee). Biogirlsa, my time at the University would not have been the same without you and I am so grateful for our unique friendship. Mamma, Pappa and Eugen you are my favorite herd.

Alexandra Isabel Sveinsen Treimo
Oslo, June 2018

Sammendrag

Nanopartikler er definert som partikler i størrelsen 1 nm til 100 nm i en dimensjon. Nanopartikler finnes naturlig i sand, glass og stein. I tannbehandlinger benyttes ofte silikananopartikler for å gi ulike materialer ønskelige egenskaper slik som polerende effekt av tannkrem, endret viskositet samt forbedrede mekaniske egenskaper i resinbaserte kompositter. Kunnskapen om potensielle uønskede effekter av partikler frigjort fra disse nanomaterialene er fremdeles mangelfull. Studier har vist at pasienter kan eksponeres for nanopartikler ved polering, sliping, utskiftning og slitasje av kompositter. Forsking viser at slike partikler kan krysse blod-hjerne barrieren og dermed havne i sentralnervesystemet. Nervesystemet er sensitivt for skader, og nevrotoksiske effekter kan ha alvorlige følger. Ved økt bruk av denne typen materialer er eksponeringsfaren for tannhelsepersonell og pasienter et økende problem. I dette *in vitro* studiet har vi benyttet PC12 celler for å studere effektene av disse silikananopartiklene. Våre funn viser at silikananopartikler endrer cellemorfologien på flere ulike måter samt reduserer celleoverlevelsen. Undersøkelser av celledød viste både apoptotiske og nekrotiske celler. Annen forskning har vist økte nivåer av reaktive oksygenforbindelser (ROS) i celler som har blitt eksponert for nanopartikler. Vi fant ingen signifikante endringer i ROS-nivåer i våre celler. For å karakterisere variasjon i respons til nanopartikler innad i en cellelinje, ble to ulike kloner av PC12 celler benyttet.

Abstract

Nanoparticles are defined as particles in the size of 1 nm to 100 nm in one dimension. Nanoparticles are found naturally in sand, glass and stone. In dental treatments, silica nanoparticles are often used to give different materials desirable properties such as the polishing effect of toothpaste, altered viscosity and improved mechanical properties in resin-based composites. The knowledge of potential undesired effects of particles released from these nanomaterials is still inadequate. Studies have shown that patients can be exposed to nanoparticles by polishing, grinding, replacing and tearing of composites. Research shows that such particles can cross the blood-brain barrier and thus end up in the central nervous system. The nervous system is sensitive to damage, and neurotoxic effects can have serious consequences. With increased use of this type of material, the dangers of dental personell and patient exposure are an increasing problem. In this in vitro study we have used PC12 cells to study the effects of these silica nanoparticles. Our findings show that silica nanoparticles change cell morphology in several different ways, and reduce cell viability. Investigations of cell death showed both apoptotic and necrotic cells. Other research has shown increased levels of reactive oxygen species (ROS) in cells exposed to nanoparticles. We found no significant changes in ROS levels in our cells. To characterize variation in response to nanoparticles within a cell line, two different clones of PC12 cells were used.

Abbreviations

Ab	Antibody
ANOVA	Analysis of variance
APS	Ammonium persulphate
ATCC	American Type Culture Collection
bp	Base pairs
CNS	Central Nervous System
CW	Center wavelength
dH2O	Distilled water
DMEM	Dulbecco's Modified Eagle Medium
DMSO	Dimethyl sulfoxide
e. g.	*exempli gratia*
Et al.	*Et alii* (and others)
EtOH	Ethanol
FBS	Fetal bovine serum
g	Gram
h	Hour
HEMA	2-hydroxyethylmethacrylate
HO-1	Heme oxygenas-1
HOECHST	2'-[4-ethoxyphenyl]-5-[4-methyl-1-piperazinyl]-2,5'-bi-1H-benzimidazole trihydrochloride trihydrate
IgG	Immunoglobin G
J	Joule
kDa	Kilo Dalton
µg	Microgram
mg	Milligram
min	Minutes
µL	Microliter
mL	Milliliter
MTT	3-(4,5-dimethylthiazol-2-yl)-2,5-disphenyltetrazolium bromide
mW	Molecular weight

n	Number of samples
Na	Sodium
NGF	Nerve growth factor
NIOM	Nordic Institute of Dental Materials
nm	Nanometer
NP	Nanoparticle
PBS	Phosphate-buffered saline
PFA	Paraformaldehyde
PI	Propidium iodide
ROS	Reactive oxygen species
rpm	Rounds per minute
SD	Standard deviation
SDH	Succinate dehydrogenase
SDS	Sodium dodecyl sulphate
SiNP	Silica nanoparticle
TBS	Tris buffered saline
TBS-T	Tris buffered saline with Tween
TEMED	N,N,N,N´,N-tetramethyl-ethylendiamine
UiO	University of Oslo

Table of contents

Acknowledgements ..... **IV**

Sammendrag ..... **V**

Abstract ..... **VI**

1 Introduction **2**
1.1 Biomaterials **2**
1.1.1 Dental biomaterials 2
1.1.2 Nanomaterials 2
1.1.3 The nervous system 4
1.1.4 Blood-brain barrier 4
1.1.5 Neurons 5
1.2 Biological responses to nanoparticle exposure **6**
1.2.1 Changes in cell morphology 6
1.2.2 Oxidative stress 6
1.2.3 Heme oxygenase-1 7
1.2.4 Cell death 8

2 Aims of the study **10**

3 Materials and methods **11**
3.1.1 Cell culture 11
3.1.2 Seeding of cells 13
3.1.3 Silica nanoparticle exposure 13
3.1.4 Assessment of cell viability 15
3.1.5 Cell death classification 16
3.1.6 Qualitative observation of cell morphology 17
3.1.7 Neurite outgrowth staining kit 18
3.1.8 Intracellular ROS measurements 19
3.1.9 Western blot analysis 21
3.1.10 Statistical analysis 23

4 Results **25**
4.1 Cell viability and cell death **25**
4.1.1 Cell viability 25
4.1.2 Apoptosis & necrosis 26
4.2 Cell characterization **28**
4.2.1 Morphological changes 28
4.2.2 Neurite outgrowth 32
4.3 Oxidative stress **33**
4.3.1 Intracellular ROS 33
4.3.2 Western blot 35

5 Discussion **37**
5.1.1 Decreased cell viability and increased cell death 37
5.1.2 Silica nanoparticles induces morphological changes in PC12 cells 38
5.1.3 The effect of silica nanoparticles on ROS levels and oxidative stress 39
5.1.4 ATCC and subclone cells gives different results 40
5.1.5 Nanoparticles in dentistry 41

6 Conclusions **42**

7 Future perspectives **43**
References **44**
Appendix **48**

1 Introduction

1.1 Biomaterials

Biomaterials are used to replace a part of an organism to retain its function. They are used in medical treatments e.g. to replace bone plates, heart valves, and in dentistry to restore teeth and enhance esthetics (Anusavice, Phillips, Shen, & Rawls, 2013; Fan, Fu, Yu, & Ray, 2014; Hildebrand Hartmut, 2013; Zhu, Wang, Lin, Xie, & Wang, 2014). It is known that biomaterials may cause side effects when inserted into the body (Williams, 1987).

1.1.1 Dental biomaterials

Dental biomaterials can be composed of metals, ceramics, polymers or composites, and are classified as preventive, restorative or auxiliary materials (Anusavice et al., 2013). These materials might cause local adverse effects in the oral cavity as well as dispersion throughout the body depending on component release, exposure time, distribution through tissue or blood, and the concentration of the component (Anusavice et al., 2013). One of the most important classes of restorative materials used in dentistry is resin-based composite. These materials mainly consist of inorganic filler particles embedded in an organic polymer matrix. The composites replaces lost teeth tissue from trauma or caries (Van Landuyt et al.). Filler particles in resin-based composites give varying physical and mechanical properties to the material, depending on the composition, size and amount of the particles (Schmalz & Arenholt-Bindslev, 2009). Large amounts of silica nano-filler are found in these composites, and it is assumed that inhalation of these particles are hazardous (Van Landuyt et al.).

1.1.2 Nanomaterials

The European Commission (2016) defines nanomaterials as "natural, incidental or manufactured material containing particles, in an unbound state or as an aggregate or as an agglomerate and where, for 50 % of more of the particles in the number size distribution, one or more external dimensions is in the size range 1 nm – 100 nm". Some common objects are illustrated on a nanometer scale below (Fig. 1).

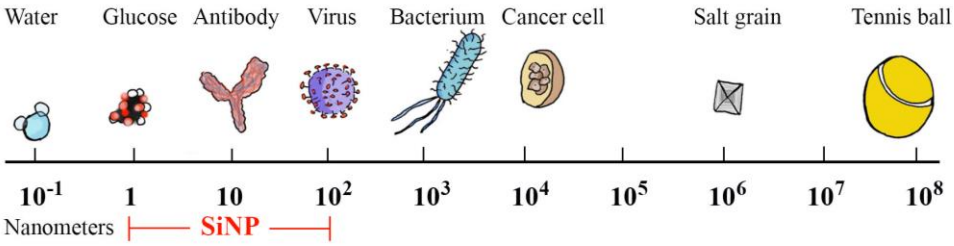

Figure 1: *Comparison of known objects on a nanometer scale. Silica nanoparticles are marked with red (1-10^2 nm). © Alexandra Isabel Sveinsen Treimo*

Silica nanoparticles (SiNPs) are one of the most commonly used components in dental materials, where they are used to obtain desired properties. In resin-based composites, SiNPs are added to improve mechanical properties and give desired viscosity (Schmalz & Arenholt-Bindslev, 2009). In toothpaste, these particles are added to give the desired grinding effect (Van Landuyt et al.). Nano-filler particles used in dentistry are range from 5 nm-100 nm. In addition, nanoaprticles are formed from brushing, polishing and natural tearing of the teeth. Shaping, polishing and removal of composite restorations aerolises composite dust. Exposure and thereby subsequent following absorption may occur through inhalation, swallowing, and absorption through the oral cavity and the mucous membranes (Schmalz & Arenholt-Bindslev, 2009). Studies have shown that inhaling silica nanoparticles may have severe adverse effects such as lung cancer, silicosis and bronchitis (Anusavice et al., 2013). SiNPs occur naturally in rocks, glass and sand, and they have extensive applications in biomedical and biotechnical fields due to their large surface to volume ratio, relatively low cost and excellent biocompatibility (Fu, 2014). Another important application of SiNPs is in drug delivery, and in targeted cancer treatment (Tang & Cheng, 2013; Wu, Wang, Sun, & Xue, 2011). The molecular characteristics of the nanoparticles are similar to important components of the cell such as DNA, proteins and other biological molecules, which makes them highly bioavailable (Feng, X. et al 2015). Investigating the possible neurotoxic effects of exposure to nanoparticles is important to ensure safe use. With increased use of nanoparticles in dentistry, dental personnel and patients are more likely to be exposed (Van Landuyt et al.). Although the use of nanomaterials has a positive effect on mechanical properties, the biosecurity of the use of nanomaterials are not fully investigated yet (He, Weiwei, Liu,

Wamer, & Yin, 2014; He, Xiaojia, Aker, Leszczynski, & Hwang, 2014; Khalili, Jafari, & Eghbal, 2015; Mirshafa, Nazari, Jahani, & Shaki, 2017).

1.1.3 The nervous system

The nervous system is responsible for storage of memories, communication to the muscles and for an organism's ability to act in the most optimal way in response to its surroundings. It is anatomically divided into the peripheral nervous system (PNS) and the central nervous system (CNS) (Brodal, 2013). The brain and the spinal cord make up the CNS, while the peripheral nervous system is outside the brain- and spinal cord membranes. The peripheral nervous system connects the CNS to the rest of the tissues in the body. Nanoparticles have potential to locate in the central nervous system (CNS), where they may be neurotoxic (Feng et al., 2015; Wu et al., 2011).

1.1.4 Blood-brain barrier

The blood-brain barrier (BBB) limits the access of neurotransmitters and toxins to the CNS. Tight junctions between brain endothelial cells create the BBB (Fig. 2), and ensure that neurotransmitters and toxins from nearby neurons are not transported directly into the blood stream in the brain (Anderson & Van Itallie, 2009; Shen et al., 2018). To pass the semipermeable blood-brain barrier, molecules has to be selectively transported by specific transporters. However, research indicates that nanoparticles smaller than 200 nm can cross the BBB directly without these transporters (Karmakar, Zhang, & Zhang, 2014; Shen et al., 2018; Song et al., 2017; Wang et al., 2011; Wu et al., 2011). It is important to map the possible effects of nanoparticles crossing the blood-brain barrier and accessing the neurons because of the irreversible effects it potentially serves. There is an ongoing discussion on whether small nanoparticles exert a stronger toxicity than larger particles (Eom & Choi, 2009).

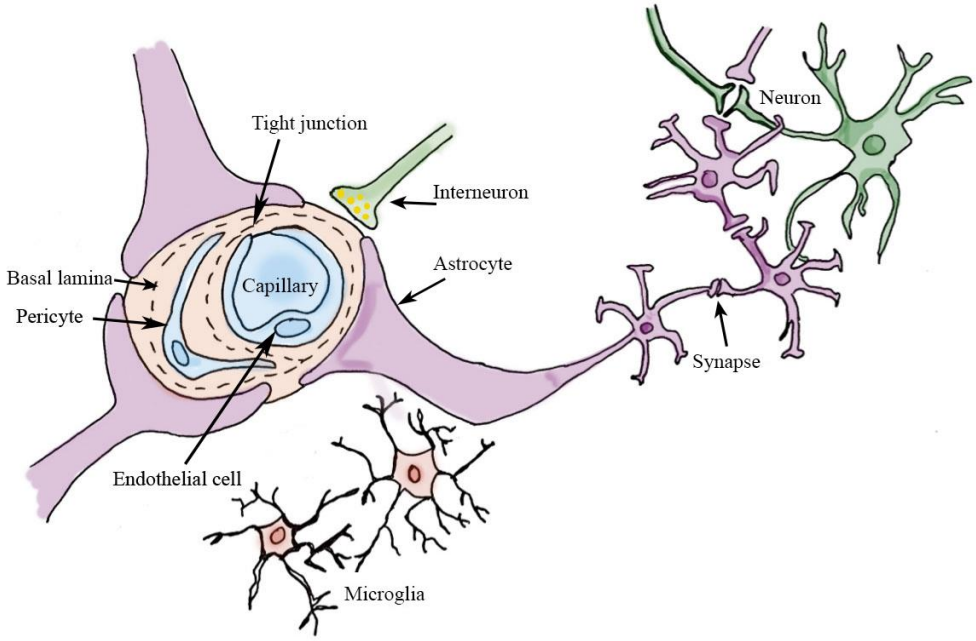

Figure 2: *Schematic drawing of the blood-brain barrier illustrating the particularly tight capillaries of the brain, surrounded by tight junctions ensuring a selective transport of compounds through the endothelial cells.* *© Alexandra Isabel Sveinsen Treimo*

1.1.5 Neurons

Neurons and glial cells are the most abundant cell types in brain tissue. They form a network that makes signaling and communication between cells possible in a highly specific and fast manner (Brodal, 2013; Wu et al., 2011). A neuron has a soma (body) with axons or dendrites branching out from the cell, covered in myelin sheath (Fig. 3).

Neurologic disorders are associated with neuronal threat or insult. Such disorders include amyotrophic lateral sclerosis (ALS), Alzheimer's disease, multiple sclerosis (MS), Parkinson's disease, Huntington's disease and stroke (Karmakar et al., 2014; Wu et al., 2011). Mechanisms behind these insults and following disorders include changes in cell morphology, oxidative stress and cell death, which inhibit the normal function of the neuronal network.

Neurotrophins is a family of signal proteins that regulates the outgrowth of dendrites and axons. The nerve growth factor (NGF) was the first neurotrophins to be discovered (Hennigan, Callaghan, & Kelly, 2007; Huang & Reichardt, 2001; Levi-Montalcini, Skaper,

Dal Toso, Petrelli, & Leon, 1996). Elevated levels of NGF are found in inflammatory and autoimmune states. It is suggested that NGF interacts with mast cells in neuro-immune systems, and that NGF serve as an alarm-molecule. NGF can be added to cell cultures and thereby promote growth of neuron like structures (Wu et al., 2011). Neurons are dependent on nerve growth factor for survival (Fujita, Lazarovici, & Guroff, 1989).

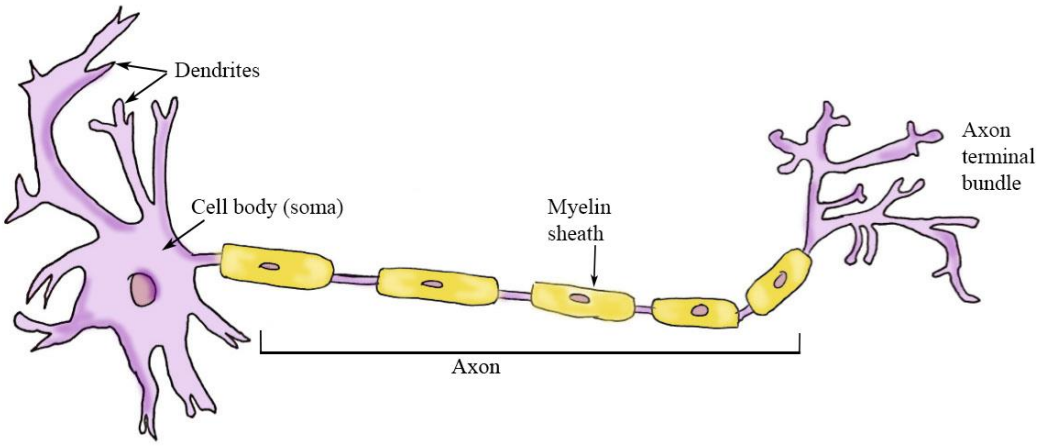

Figure 3: *Essential structures of a neuron, including dendrites, cell body (soma), the axon and axon terminal bundle. Myelin sheath covers the axon, increasing the speed of the signal. © Alexandra Isabel Sveinsen Treimo*

1.2 Biological responses to nanoparticle exposure

1.2.1 Changes in cell morphology

Changes in cell morphology after exposure to nanoparticles have been seen in various cell types, including PC12 cells (Farajalla, 2015; Khalili et al., 2015; Murugadoss et al., 2017; Oh & Park, 2014; Wang et al., 2011; Wu et al., 2011). These alterations can be seen as rounding and fragmentation of cells, vacuolization, and formation of needle-like cells. This could indicate malformations in the cytoskeletal structure, and could also be a sign of apoptotic activity in the cells (Wu et al., 2011). Injuries to neurons may have severe consequences as described in 1.1.5.

1.2.2 Oxidative stress

Nanoparticles have been shown to induce oxidative stress in various cell types (Eom & Choi, 2009; Fu, Xia, Hwang, Ray, & Yu, 2014). Reactive oxygen species (ROS) are natural by-products from metabolism, and are highly reactive molecules essential in cell signaling. They

serve as intra- and intercellular messengers (Hancock, Desikan, & Neill, 2001). ROS also play essential roles in other vital physiological functions such as apoptosis and gene expression (Hancock et al., 2001). Excessive production or reduced removal of reactive oxygen species disturbs the redox balance, which inhibits and disturbs the cells normal biological functions. This is referred to as oxidative stress (Fig. 6) (Aprioku, 2013; Fu et al., 2014; Murugadoss et al., 2017). Oxidative stress occurs when cellular processes and molecules such as antioxidants fail at neutralizing ROS, such as $O_2^{-\cdot}$, hydrogen peroxide (H_2O_2) and nitric oxide (NO) in a cellular system (Fig. 4). These free radicals can attack and damage proteins, nucleic acids and lipids (Hancock et al., 2001; Vincent, Russell, Low, & Feldman, 2004). Ultimately, failure to remove free radicals may initiate apoptotic or necrotic mechanisms in cells. The nervous system is particularly vulnerable to oxidative stress because the repair mechanisms for neurons in many cases is limited, although neurons may reform in some areas of the brain (Brodal, 2013).

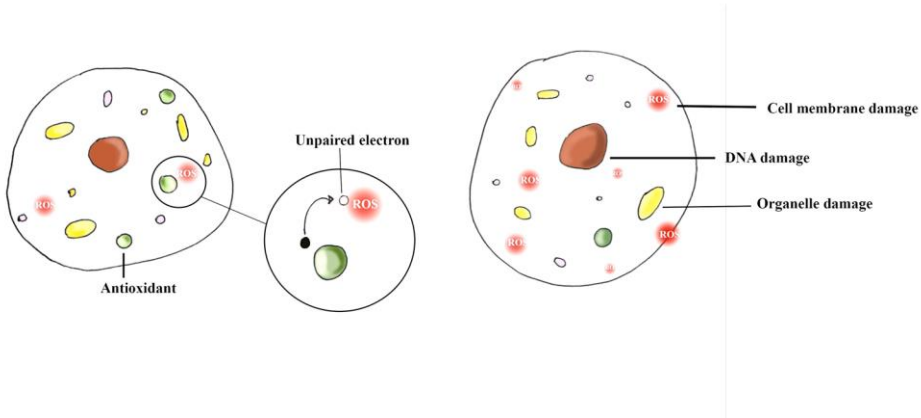

Figure 4: *Mechanism of ROS formation. Antioxidants neutralize ROS by donating an electron. The lack of antioxidants may result in more ROS and damages to cell membrane, DNA and organelles. (c) Alexandra Isabel Sveinsen Treimo*

1.2.3 Heme oxygenase-1

The enzyme heme oxygenase-1 (HO-1) has been shown to increase in response to nanoparticle exposure (Lai, 2015). It has a strong neuroprotective function, and is induced by a wide array of inflammatory and oxidative stress factors in the brain. Heme is degraded by HO-1 to iron, biliverdin and carbon monoxide (CO). Vasodilation (extension of blood vessels allowing bigger blood flow to inflammatory tissue), inhibition of apoptosis (controlled cell death) and mitochondrial respiration is then stimulated. Elevated levels of HO-1 could

indicate oxidative stress or an inflammatory state in cells (Calabrese, Mancuso, De Marco, Stella, & Butterfield, 2007).

1.2.4 Cell death

Cell death after exposure to nanoparticles is seen in earlier studies (Peixoto, de Oliveira Galvão, & Batistuzzo de Medeiros, 2017). Based on morphological criteria, cell death has traditionally been categorized as either apoptosis or necrosis. Today, several different subcategories of apoptosis and necrosis are used (Hotchkiss, Strasser, McDunn, & Swanson, 2009; Yamaguchi & Miura, 2015). These subcategories have not been fully investigated. Therefore the simplified categorization into apoptosis and necrosis is still useful and widely used to give an overview of the mechanisms behind cell death.

Apoptosis, also referred to as regulated cell death, is activated by either internal or extracellular signals. It was first introduced by Kerr et al. in 1972 (Kerr, Wyllie, & Currie, 1972). The terminal stages of cell death is characterized by formation of cell membrane blebbing, cell shrinkage, DNA fragmentation and chromatin condensation resulting in the formation of apoptotic bodies (Fig. 5) (Asweto et al., 2017). Extrinsic pathways are caused by extracellular signals such as a virus infection. In this case, death receptors are activated by the binding of a ligand to the receptors of the surface, which in turn activates a cascade of events eventually leading to apoptosis. Independent on the source of signal, the cell shrinks and becomes more spherical due to the internal destruction of nucleus and the cytoskeleton in the apoptotic cell. The plasma membrane then forms irregular extensions forming blebs, developing fragments that break away from the cell (Fig. 5). Phagocytic cells then engulf these fragments.

Necrosis is cell death caused by external factors, and is sometimes referred to as spontaneous cell death (Majno & Joris, 1995). As for the apoptosis, several types of necrosis are suggested to exist. Common for necrosis is cell and organelle swelling and membrane rupture followed by the release of intracellular content (Cummings Brian & Schnellmann Rick, 2004).

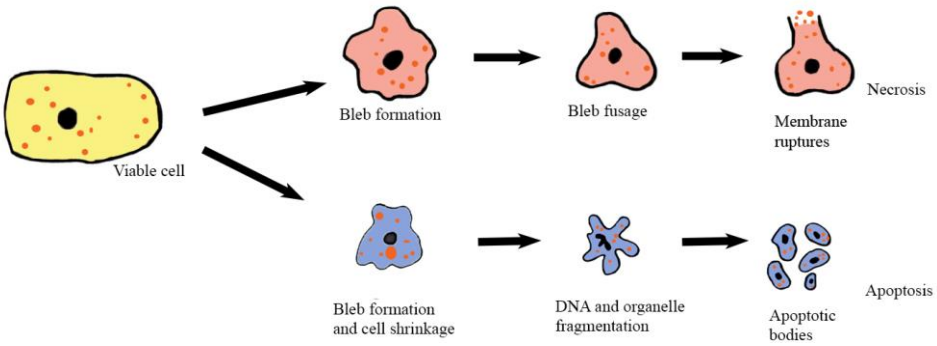

Figure 5: *Simplified schematic drawing of necrotic and apoptotic cell death © Alexandra Isabel Sveinsen Treimo*

2 Aims of the study

The aim of this master project was to gain knowledge about the possible neurotoxic effects of nanoparticles used in dental materials. To address this over-all aim, the following six objectives were set for our study:

- To test if silica nanoparticles reduces cell viability in exposed PC12 cells
- To test if silica nanoparticles induces apoptosis and necrosis in exposed PC12 cells
- To test if silica nanoparticles will induce morphological changes in exposed PC12 cells
- To test if silica nanoparticles induces oxidative stress responses in exposed PC12 cells
- To test if the toxic potential of SiNP 10 nm is higher than for SiNP 50 nm in PC12 cells
- To test if the cell clones ATCC and subclone give the same responses to silica nanoparticle exposure

3 Materials and methods

The experimental design covers effects of nanoparticles on cell morphology, oxidative stress, heme oxygenase-1 and on cell viability and cell death (Fig. 7).

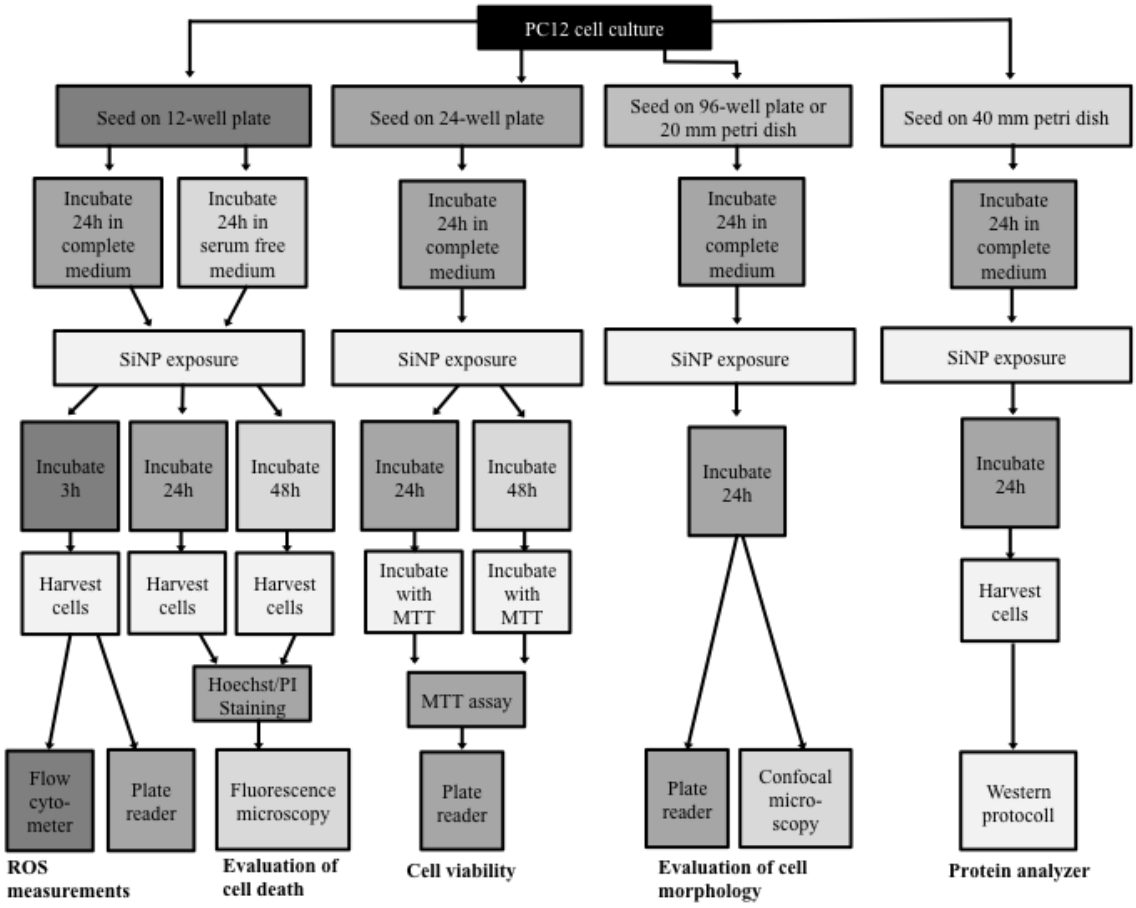

Figure 6: *Experimental design for in vitro experiments used to study effects of silica nanoparticles on exposed PC12 cells.*

3.1.1 Cell culture

Toxicity was measured with different assays (Fig. 6) to determine the effects of SiNP exposure on PC12 cells. The cells were seeded out and incubated for 24h, before exposure to different concentrations of SiNP 10 nm and SiNP 50 nm.

In this *in vitro* study, the PC12 cell line was used as a model for nerve cells because of its ability to form neuron like structures (de los Rios, Cano-Abad, Villarroya, & López, 2017; Greene & Tischler, 1976; Radio & Mundy, 2008). This makes it possible to study potential

neurotoxic effects when exposed to silica nanoparticles. The PC12 cell line is well studied, and has been used in similar studies (Migliore, Uboldi, Di Bucchianico, & Coppedè, 2015; Radio & Mundy, 2008; Wang et al., 2011). These cells are collected from the adrenal gland in rats, from pheochromocytoma, a tumor arising from chromaffin cells of the adrenal medulla (Schimmelpfeng, J. et. al 2004). We used two different clones of PC12 cells, the ATCC and the subclone. The ATCC cells were purchased October 2016, and the subclone cells were kindly provided by Ragnhild Paulsen's laboratory at Institute of Pharmacy at the University of Oslo. Both the ATCC and subclone cells are adherent. Subclone cells were originally cloned to respond to nerve growth factor and to be adhesive.

The PC12 cells used in this study were grown adherently in culture medium at 37°C in a humidified incubator containing an atmosphere of 5% CO_2. Significance of cell batch and passage number was examined.

Procedure

Cells were stored in liquid nitrogen until use. Before cell culturing, cells were defrosted in a water bath at 37°C. The cells were grown in suspension in a non-coated 75cm^2 cell culture flask. Splitting of cells was done two to three times a week, depending on cell confluency. Old growth culture medium was discarded using a suction pipette. To remove dead cells and debris from old growth culture medium, 10 mL PBS (Phosphate-buffered saline) was carefully added. PBS was removed before adding 10 mL fresh complete cell culture medium to cell culture flask. To dissociate adherent cells from the cell culture flask, either manually agitated, enzymatically dissociated by trypsin or mechanically detached by cell scraper. To homogenize the cell culture, cells were carefully pipetted repeatedly. Homogenous cell culture solution (1.5 mL) was added to a new cell culture flask and mixed with 20 mL complete cell culture medium. The cells presence were observed using a phase contrast microscope, and subsequently incubated at stable 5% CO_2 atmosphere and 37°C. All work was performed under sterile conditions.

Various constituents were defrosted and vortexed before they were added to 500 mL DMEM to make serum-free and complete culture medium (Table 1).

Table 1: *Constituents of complete and serum-free medium used in all models *denotes serum only included in complete cell culture medium*

Constituents	Amount
DMEM, sterile filtrated from the fabricant	500 mL
Horse serum, not sterile filtrated	25 mL *
Calf serum, not sterile filtrated	50 mL *
Glutamine, sterile filtrated from the fabricant	5 mL
Penicilin-Streptomycin, sterile filtrated from the fabricant	5 mL
Na Pyruvate, sterile filtrated from the fabricant	5 mL

3.1.2 Seeding of cells

The cell density (cells/mL) was obtained by applying 75 µL diluted cell suspension in MOXI Z Mini Automated Cell counter. The desired cell density, 40 000 cells per mL culture medium, was calculated as presented under (Equation 1).

$$Conc_{desired\ cd} \times Vol_{medium} = Conc_{actual\ cd} \times Vol_{cs}$$

Where $Conc_{desired\ cd}$ = concentration of desired cell density (µg/mL), Vol_{medium} = volume culture medium (mL), $Conc_{actual\ cd}$ = actual cell density counted (µg/mL) and Vol_{cs} = volume cell suspension (mL).

Cell density in 12 and 24 well plates as well as the 40 mm culture dishes was 40 000 cells/mL culture medium. The 96 well plates had a cell density of 4000 cells/mL. 1 mL culture medium was added to each well of the 12 and 24 well plates. To the 96 well plates, 100 µL culture medium was added to each well, and to the 40 mm culture dishes we added 3.5 mL (Fig. 6). All plates and dishes were incubated in a humidified atmosphere at 37°C with 5% CO_2 for 24 hours.

3.1.3 Silica nanoparticle exposure

The same round silica nanoparticles (SiNPs) with average sizes 10 and 50 nm as characterized by Låg and colleagues (2018) were used in this study. SiNP 10 nm agglomerate to some extent in complete culture medium while SiNP 50 nm is monodisperse (Fig. 7).

A (SiNP 10 nm) **B (SiNP 50 nm)**

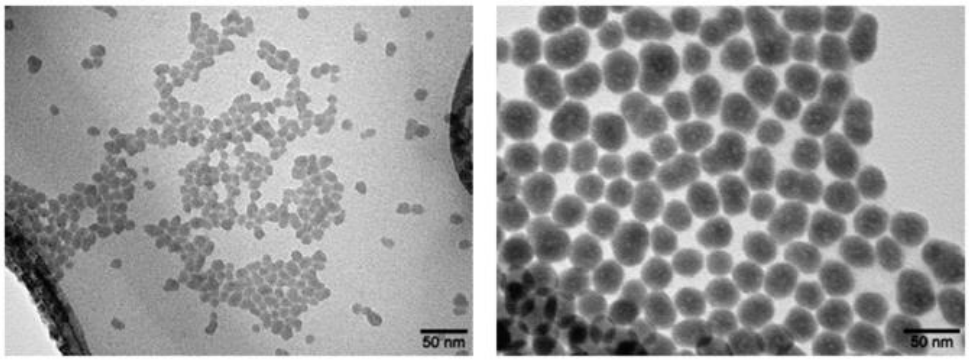

Figure 7: A) SiNP 10 nm, B) SiNP 50 nm. Pictures are taken with TEM micrographs using JEM 1400 (Jeol, Japan). Scale bar: 50 nm. Particles are non-crystalline mono disperse silica nanoparticles. Pictures used with permission from Marit Låg and colleagues. (Låg et al., 2018)

PC12 cells were exposed to 10 nm or 50 nm silica nanoparticles, and was selected based on the particles added to dental composite fillings (Anusavice et al., 2013). Stock solutions were prepared and dispersed to the different samples following the procedure described below. Because silica nanoparticles are known to cluster, Låg and colleagues (2018), sonicated and treated the silica nanoparticles with bovine serum albumin prior to exposure to avoid clustering in their studies. It is reason to believe that the particles used in this study share the same characteristics, as the same protocol was followed. Another application done to avoid clustering was to expose cells in serum-free medium. In this way coating of the particles by proteins does not occur. An estimate of what concentrations dental personnel and patients are exposed to is challenging. The concentration of silica nanoparticles used was therefore selected based on earlier studies (Farajalla, 2015)

Procedure

SiNP 10 nm and SiNP 50 nm particle stock solutions were disperesed in dH_2O (2.3 mg/ml) and sonicated until specific ultrasound energy of 180 J was given to the nanoparticles. After sonication, 34.5 μL BSA (in dH_2O 50 mg/mL) and 115 μL PBS was added to each tube. Final concentration in exposure stock solution was 2 mg/ml.

Table 2: *SiNP 10nm and 50 nm exposure concentrations used in experiments. Complete and serum free culture medium (controls) was made according to table 1.*

	Concentrations						
SiNP (µg/mL)	3.125	6.25	12.5	25	50	Complete medium	Serum-free medium

All assays used the following equation (Equation 2) to calculate the concentrations described in table 2:

$$Vol_{NP} = \frac{Vol_{Conc} \times Vol_{Total\ conc}}{Density}$$

Where, Vol_{NP} = volume nanoparticle solution (mL), Vol_{Conc} = volume concentration (µg/mL), $Vol_{Total\ conc}$ = total amount needed per concentration (mL) and *Density* = 2000 µg/mL.

3.1.4 Assessment of cell viability

To measure cell survival and proliferation (cell viability), the MTT (3-[4,5-dimethylthiazol-2-yl]-2,5 diphenyl tetrazolium bromide) assay was used. Yellow MTT substrate is transformed to purple formazan crystals by the mitochondrial membrane bound enzyme complex succinate-dehydrogenase (SDH) (Fig. 8). SDH is only active in viable cells, and therefor the number of viable cells in a sample is reflected by the amount of produced formazan, detected by measuring the absorbance using the plate reader Synergy H1 Hybride Reader by BioTek.

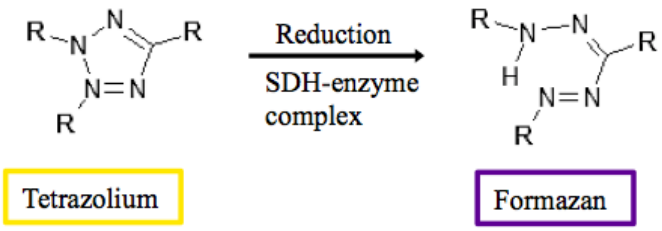

Figure 8: *The membrane bound mitochondrial SDH-enzyme complex reduces tetrazolium (yellow MTT dye) to formazan (purple). The MTT substrate is only active in viable cells. Formazan crystals are only formed in viable cells, and can be used to quantify the amount of viable cells in a sample.*

Procedure

Prior to exposure, pictures were taken using Olympus Camedia C-7070 in the CKX41 phase contrast microscope by Olympus. Old medium was removed after incubation. 500 μL PBS was added to each well and removed before adding 500 μL NP solution according to equation 2. Cells were incubated for 24h and 48h at a stable 37°C and 5% CO_2. After exposure and incubation for respectively 24 or 48 hours, old medium was removed. 400 μL MTT solution consisting of 1 mL MTT stock solved in 9 mL PBS was added per well in a 24-well plate. Incubation followed at 37°C, 5% CO_2 for 1 hour. MTT-solution was removed and 400 μL DMSO was added to each well. To dissolve the formazan crystals, plates were shaken for 10-15 minutes. Prior to analyzing the samples in a multiwall scanning spectrophotometer, 200 μL of the dissolved solution from each well at the 24-well plate was added to 24 wells in a 96-well plate.

3.1.5 Cell death classification

Cells were stained using the fluorochromes HOECHST and PI, to classify cell death by fluorescence microscopy. Viable, apoptotic and necrotic cells were counted. The cell membrane is stained differently based on the integrity of the membrane. PI stains DNA in cells with non-intact membranes, while HOECHST stains DNA in all cells. Apoptotic and viable cells are both blue, but as the DNA is condensed in apoptotic cells, the stain is more intense in these cells (Fig. 9). Necrotic cells are colored red (Fig. 9). This method is well established and can be adjusted to fit a numerous different cell types and toxicants (Cummings Brian & Schnellmann Rick, 2004). As the results depend a lot on practice to accurately define the different structures, careful consideration of the results must be done (Cummings Brian & Schnellmann Rick, 2004).

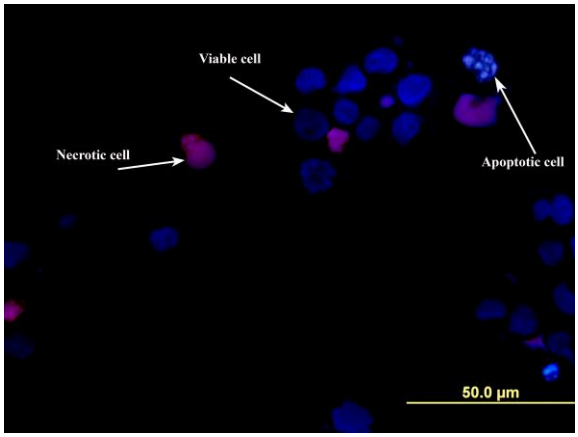

Figure 9: *Fluorescence microscopy picture of necrotic, apoptotic and viable cells stained with Propidium and Hoechst 33342. Viable cells are shown as less intense blue cells than the apoptotic cells. Necrotic cells are stained red.*

Procedure

After incubating and exposing samples (see 3.1.1-3.1.3), old culture medium was removed and transferred to a new micro tube together with culture medium. Cell culture dishes were washed two times with 200µL Trypsin. The trypsin wash residues were added to an eppendorf tube together with culture medium. 100µL Trypsin was added to each cell dish and incubated 3-10 min at stable 5% CO_2 and 37°C until the cells were loose. When cells were detached, the samples were added to the eppendorf tubes in the previous step and then centrifuged 10 min, 250 g.

Supernatant was then removed and 50 µl of the serum with Hoechst 33342/PI (500 µL serum with 5 µL Hoechst 33342 (10µg/µL) and 5µL PI (10µg/µL) was added to the pellet in each tube. Incubation followed protected from light for 30 min at room temperature. One drop was then pipetted onto a microscope slide and spread out using a clean microscope slide. Slides were dried in room temperature and protected against light before studied using a florescence microscope (filter 4, 100x magnitude with oil). A minimum of 300 cells was counted from each sample, categorizing viable, apoptotic and necrotic cells.

3.1.6 Qualitative observation of cell morphology

To study cell morphology, a phase contrast microscope was used. Pictures were taken at 20x magnification after 24h and 48h exposure to varying concentrations of nanoparticles. Controls with complete medium and serum-deprived medium were used for comparison.

Confocal microscopy was also used to investigate changes in cell morphology. Adobe Photoshop CS6 version 13.0 x64 was used to analyze the pictures at a 50 μm scale.

3.1.7 Neurite outgrowth staining kit

First, several attempts at using the neurite outgrowth staining kit to quantify changes in cell surface in silica nanoparticle exposed cells was done. As the kit failed to detect differences between NGF-treated cells (with clearly visible neurite outgrowth), and controls (without neurites), we used the kit for confocal microscopy to study cell morphology in silica nanoparticle exposed cells. This kit dyes the cell membrane giving the membranes fluorescent properties. Exposed cells were studied and photographed using Olympus FV1000 confocal laser scanning biological microscope.

Procedure

Cells were counted and seeded as described in 3.1.1 and 3.1.2. Initially, 96-well plates were used to measure the surface area of the cells, while 20 mm cell dishes were used to analyze the cells in confocal microscopy.

96-well plates:

100 μL cell suspension was added to each well in the 96-well plate and subsequently incubated in a humidified atmosphere at 37°C with 5% CO_2 for 24 hours. Nerve growth factor (NGF) solution (1:100) was prepared (Table 3).

Table 3: *Preparation of NGF solution, dilution 1:100.*

Constituents	**Amount**
NGF (10μg/mL, diluted in serum-free medium)	40 μg
Complete medium	4 mL

Nanoparticle solutions were made as described in 2.1.4. Old medium was carefully removed and 100 μL PBS was added and discarded before exposure. Cells were exposed one well at a time to avoid the cells to dry out. Cells were incubated at 37°C, 5% CO_2 for 24 hours. Phase contrast microscopy was used to look for morphological changes, and pictures were taken for later comparison. Incubation was repeated at 37°C, 5% CO_2 for 24 hours. Phase contrast microscopy was used to look for morphological changes. Old medium was carefully removed and new complete medium was added. 10 μL cell viability indicator, 10 μL 1 x cell

membrane stain and 10 mL DPBS buffer was mixed to make a working stain solution. 100 µL of this working stain solution was added to each of the wells and incubated for 10-20 minutes. Before adding 100 µL 1 x working solution background suppression stain, consisting of 10 mL DPBS buffer and 100 µL background stain, the 1 x cell membrane stain was removed (Appendix 6, Table 7). Samples were analyzed using a fluorescence plate reader.

20 mm cell plates:

Samples were prepared following the same protocol as described above, after adjusting volumes to 20 mm cell plates. Pictures were taken in the phase contrast microscope for later comparison. Cell density was 30000 cells/mL. Before analyzing the samples in confocal microscopy, 1.5 mL 1 x fix/stain solution was added to each well and incubated 10-15 minutes. After incubation, 1.5 mL 1 x working solution background suppression dye was added to each well.

3.1.8 Intracellular ROS measurements

Reactive oxygen species (ROS) was measured in silica nanoparticle exposed PC12 cells by measuring a fluorescent compound. Two different methods were used on the samples. The flow cytometer uses scattered light and fluorescent labeling to analyze single cells while they are passing by the light source in the samples. The other method also reads fluorescence in the sample by illuminating and emitting light at a specific wavelength; however this was carried out by a plate reader. Two types of cellular reactive oxygen species detection assay kits were used. The probes 5-(and-6)-chloromethyl-2',7'-dichlorofluorescin diacetate (CM-H_2DCFDA) and dihydrorhodamine 123 (DHR) measure different types of reactive oxygen species. CM-H_2DCFDA is a fluorogenic probe that measures hydroxyl, peroxyl, hydrogen peroxide and other reactive oxygen species within the cell. When crossing the cell membrane, DCFDA is intracellular deacetylated by esterases, and becomes non-fluorescent (Sun et al., 2011). By oxidation of ROS, the highly fluorescent compound DCF is made (Fig. 8). DCF is only detectable in live cells, and has an excitation and emission spectra between 495 nm and 529 nm.

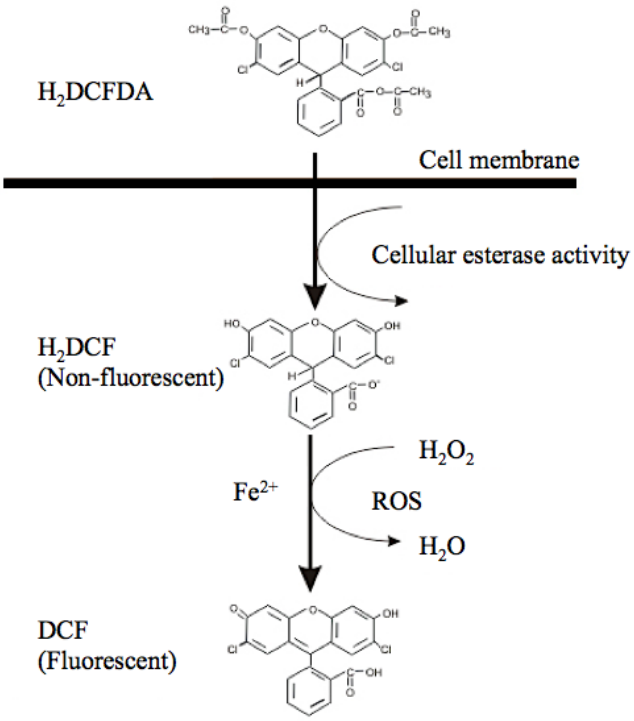

Figure 10: *H_2DCFDA diffuses across cell membranes where it is deacetylated by cellular esterases to the non-fluorescent compound H_2DCF. Reactive oxygen species oxidizes this non-fluorescent compound into the highly fluorescent compound DCF that is detected in the flow cytometer or the plate reader*

The second probe used was dihydrorhodamine 123 (DHR), and is similar to the CM-H_2DCFDA, a cell-permeable fluorogenic dye. It measures peroxide, peroxynitrite, superoxide and hydrogen peroxide. DHR is non-fluorescent and is oxidized by ROS after crossing the cell membrane (Fig. 11). Fe^{2+} is required to oxidize DHR to the fluorescent compound rhodamine 123. DHR is only detectable in live cells, and has an excitation and emission spectra between 500 nm and 536 nm.

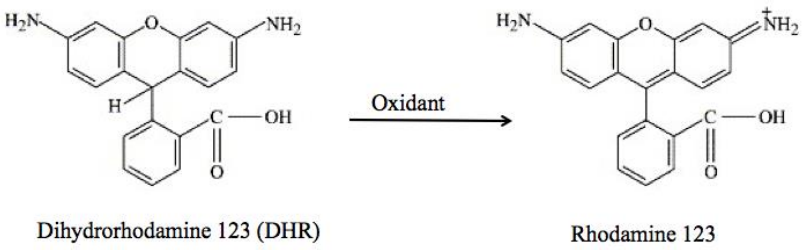

Figure 11: *The non-fluorescent compound dihydrorhodamine 123 (DHR) diffuses across cell membranes where it is oxidized by reactive oxygen species into the highly fluorescent compound rhodamine 123 detected by the flow cytometer or the plate reader*

Procedure

Cells were grown on 12-well plates for 24 hours prior to exposure. Desired cell density was 40 000 cells/mL, and 1 mL cell suspension with nanoparticle solution was added to each well after removing old culture medium with serum and washing with PBS (Equation 1 and 2). Cells were exposed for 3 hours, before they were analyzed.

DCFDA-probe solution was prepared by mixing 50 μL CM-H2-DCFDA with 29 μL DMSO. 15 μL of the DCFDA-probe solution was then mixed with 135μL serum-free culture medium. DHR probe was mixed with 135 μL serum-free culture medium. 8 μL of the DCFDA solution was added to each well on one of the plates, and 10 μL of the DHR solution was added to each well on the other plate. Incubation was done for 15 minutes at 37°C and 5% CO_2. 500 μL PBS/FBS solution was added to each well on both plates after removing old solution from the samples. PBS/FBS solution consists of 140 μL Fetal Bovine Serum (FBS) and 14μL PBS mixed together. Cells were collected either by incubating UpCell plates in room temperature for 30 minutes or by agitating cells off the plates and into micro tubes. Samples were put on ice and away from light, then analyzed using Flow Cytometer.

3.1.9 Western blot analysis

Western blot is a common analysis used to separate and identify proteins using antibodies (Mahmood & Yang, 2012). Gel electrophoresis separate the different molecules based on differences in molecular weight. Different proteins are visible as bands on the gel that are subsequently transferred to a membrane. The membrane is incubated with antibodies specific to the protein of interest. Unbound antibodies are washed off, using TBS-T (Tris Buffered Saline with Tween) buffer. The thickness and intensity of the band corresponds to the amount of protein in the sample. Membranes are analyzed using Odyssey CLx Western Blot scanner.

The resin monomer 2-hydroxyethl methacrylate (HEMA) is known to disturb cell functions and enhances HO-1 expression (Krifka et al., 2012). Based on this knowledge, HEMA was used as a positive control.

Procedure

Gel electrophoresis

Samples were seeded and exposed and harvested as previously described and stored at -20°C. Stored samples were defrosted and sonicated prior to analysis (Table 4). Samples were mixed in a solution with 10 % 2-mercaptoethanol with bromphenyl blue solution, to cleave disulfide bonds and used as a tracking dye, respectively.

Table 4: *Sonicator settings to prepare western blot samples, microtip 3 mm. Sonicator was washed with dH_2O between each run.*

Time	Pulse	Amplitude	Pause
30 seconds	05	25 %	2

Separating gel was prepared (Appendix 8, Table 9). The gel solution (7 mL) was applied between the glass plates in Mini-Protean Tetra Cell casting frame. To avoid drying of the gel, distilled water was added on top of the gels. The gels were ready after 30 minutes. Stacking gel was made and 2 mL were added on top of the separating gel after removing excess water (Appendix 6). Combs to make wells for the samples were added. Gels were set in 30 minutes. When the gels had set, they were mounted in cell casting frame for gel electrophoresis. Combs were removed. SDS-PAGE running buffer (Appendix 8, Table 8) was added before 2 μL loading marker was added to the first well of each gel. To the remaining wells, 12 μL of the samples were applied. The electric current (Ampere) was set at a constant corresponding to 100 Volt, and electrophoresis ran for 1-1.5 hours in room temperature. Electrophoresis was stopped when the front marker had nearly reached the end of the gels.

Protein transfer

Transfer buffer with methanol was made (Appendix 8, Table 8). Each gel was placed on top of a nitrocellulose membrane with 3 mm filter paper soaked in transfer buffer with methanol. To avoid air bubbles in the gel, a rolling pin was used. Before closing the gel holder cassette and mounting it for electrophoresis, black pads were added on each side of the filter paper. The gel holder cassette was placed in an electrophoresis chamber and put on ice. Transfer buffer with methanol was added. Voltage was set to constant 35V and run over night.

Ponceau S staining

Membranes were stained with Ponceau to rapidly stain protein bonds. After staining, the light sensitive membranes were kept in the dark to dry. Infrared pen was used to name and mark the membranes.

Blocking and detection of proteins

Membranes were blocked in 5 mL 5% skim milk solution in the dark on a tilting machine for 30 minutes.

Table 5: *Preparation of 5 % skim milk solution*

Constituents	**Amount**
Skim milk powder	2.5 g
TBS-T 1x Tris with Tween	50 mL

Membranes were incubated with primary antibodies of interest, mixed with 5% skim milk solution in TBS-T 1x Tris with Tween (Appendix 8, Table 8) and incubated at 4°C overnight. The following day membranes were washed with cold TBS-T solution 3x5 min on tilting machine. Subsequently, the membranes were incubated with secondary antibody for 1-2 hours at room temperature (Appendix 8, Table 10). Secondary antibody was diluted according to table x and mixed with skim milk solution. After incubation, membranes were washed with cold TBS-T solution 3x5 min. Membranes dried in the dark before they were analyzed at Odyssey CLx Infrared Imaging System.

3.1.10 Statistical analysis

Microsoft Excel 14.7.1 was used to normalize the data prior to statistical analysis. All values were divided by the mean value of all values in each experiment. Next step was to divide each individual value by the mean of all controls for all experiments before multiplying by 100. This gave the percentage at the same level of all experiments still maintaining the variation in the control groups. All data was normalized against serum-free control (0 μg/mL SiNP).

The results from Western blot analysis were normalized against loading control α-tubulin to ensure correct calculation of protein amount.

The GraphPad Prizm 7.0 software for Mac OS X was used to run statistical analysis on all data. Depending on the number of explanatory variables of the experiment, a one-way ANOVA test was used. Dunnett's multiple comparison test was used to compare all treatments against serum-free control. A linear relationship trend test was run on data with three or more replicates, to determine if there was a dose-response relationship. All data were presented as means ± standard deviation. The level of statistical significance was set at p-values lower than 0.05.

4 Results

4.1 Cell viability and cell death

4.1.1 Cell viability

Cell viability was investigated using the MTT-assay. Cell viability was significantly dose-dependently reduced in ATCC cells exposed for 24 and 48 hours to SiNP 10 nm 25 μg/mL and 50 μg/mL (Fig. 12 A-1 and Fig. 13 B-1). The subclone cells did not show a significant dose-dependent SDH-activity after 24 or 48 hours exposure (Fig. 12 A-2 and 13 B-2). Decreased cell viability was seen in subclone cells exposed to SiNP 10 nm 25 μg/mL and 50 μg/mL for 24 hours. A multiple comparison test showed a significant trend in ATCC exposed 24 hours and subclone cells exposed for 48 hours. No significant trend was found in ATCC cells exposed for 48 hours, neither in subclone cells exposed for 24 hours. Standard deviation was remarkably larger in subclone cells than in ATCC cells.

ATCC cells

A-1

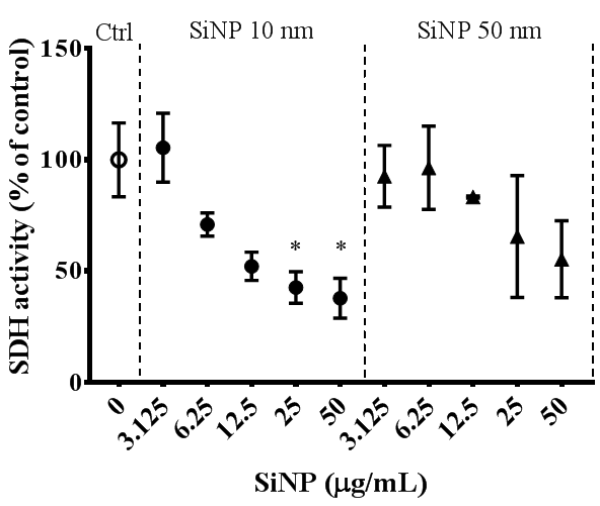

Subclone cells

A-2

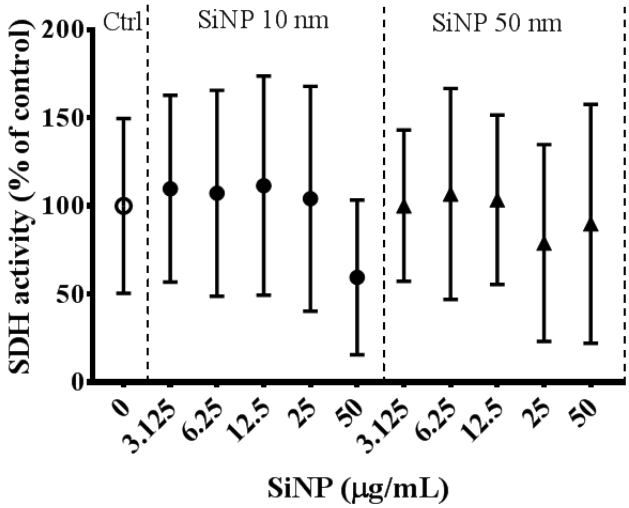

Figure 12 A-1 and A-2: *Measured SDH-activity after 24 hours of SiNP exposure, normalized to serum free control (0). A-1) ATCC cells, A-2) subclone cells. Significant difference in SDH-activity was found in control with serum in A-2 (Appendix 10). Test for linear trend was significant in A-1 (SiNP 10 and 50 nm). All statistical analysis is performed by One-way ANOVA, Dunnett's multiple comparison test and test for linear trend between column mean and left to right column order ($p \leq 0.05$ is considered statistically significant). The results are shown as mean ± SD ($n \geq 3$), *denotes significant result*

ATCC cells **Subclone cells**

B-1 **B-2**

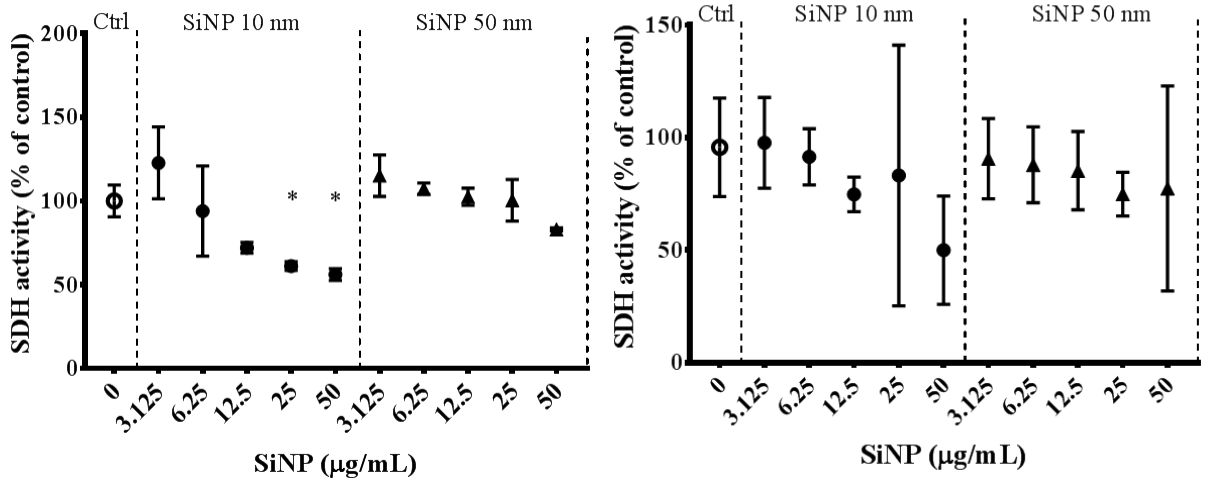

Figure 13 B-1 and B-2: *Measured SDH-activity after 48 hours of SiNP exposure, normalized to serum free control (0). B-1) ATCC cells, B-2) subclone cells. Test for linear trend was significant in B-1 (SiNP 10 and 50 nm) and B-2 (SiNP 10 nm). All statistical analysis is performed by One-way ANOVA, Dunnett's multiple comparison test and test for linear trend between column mean and left to right column order. The results are shown as mean ± SD (n=3), *denotes significant result (p≤0.05).*

4.1.2 Apoptosis & necrosis

Cells were exposed for 24 and 48 hours to varying concentrations of SiNP 10 nm and SiNP 50 nm (Fig. 14 A-2 and B-2). These experiments were only done in subclone cells. Fluorescence microscopy was used to categorize cells stained with Hoechst 33342 and Propidium iodide (PI) according to color and morphology. The number of apoptotic, necrotic and viable cells was counted.

After 24 hours, apoptotic cell death seems to be dose-dependent up to 12.5 µg/mL for the SiNP 10 nm exposed samples (Fig. 14 A-2). At the two highest concentrations, necrotic cells seemed to be most abundant. In the SINP 50 nm exposed samples, no dose-dependency was observed.

In cells exposed for 48 hours, the number of necrotic cells is remarkably higher than the apoptotic. The control also shows a high number of necrotic cells after 48 hours of exposure (Fig. 14 B-2).

Subclone cells

A-2

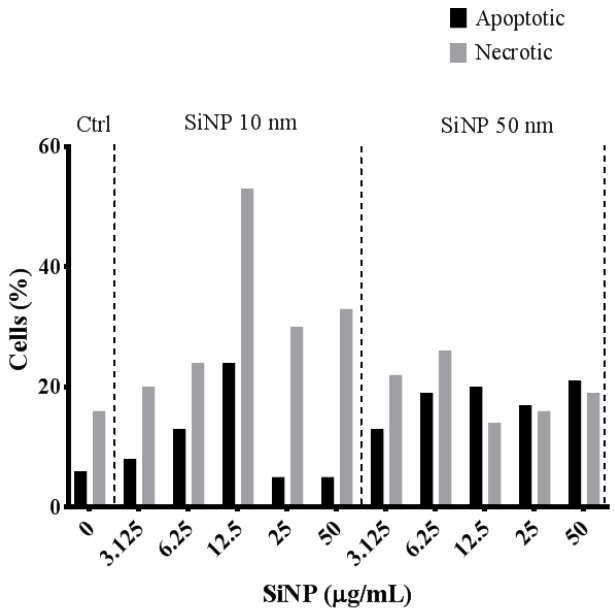

B-2

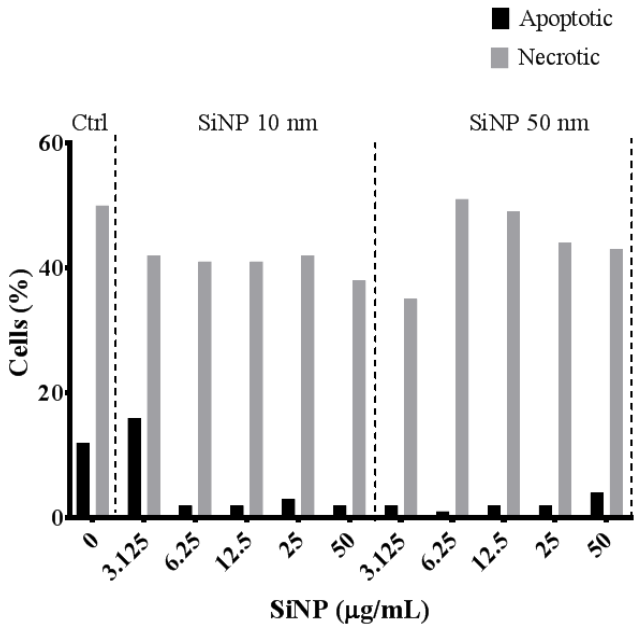

Figure 14 A-2 and B-2: *Cell death measured in subclone cells using fluorescence microscopy. Percentage of apoptotic- and necrotic cells after 24 hours (exposure to varying concentrations of SiNP 10 nm and SiNP 50 nm. At least 300 cells were counted in each sample. No statistical analysis was done (n=1).*

4.2 Cell characterization

Earlier studies have shown changes in cell morphology such as rounding, shrinkage and fragmentation of cells, and formation of needle-like structures of PC12 cells when exposed to silica nanoparticles (Farajalla, 2015; Wang et al., 2011). Effects of silica nanoparticles on these features were studied, and different responses in ATCC and subclone cells were compared.

4.2.1 Morphological changes

Phase contrast microscopy was used to visually investigate morphological changes in PC12 cells exposed to silica nanoparticles. Cells were categorized into *viable cells*, including outgrowth of neurite like structures (marked with black arrows), *damaged cells*, including spherical and fragmented cells (marked with red arrows), *needle-like structures* (marked with white arrows) and *vacuolization* (marked with blue arrows) (Fig. 15, Fig. 16 and Fig. 17). Viable cells were in majority in all control samples (Fig. 15). Cell density was similar in all control groups. Damaged cells were most profound for cells grown in serum-free medium, but were also found in cells grown in complete medium. Vacuolization was only observed in ATCC cells and not in sub clone cells (Fig. 15).

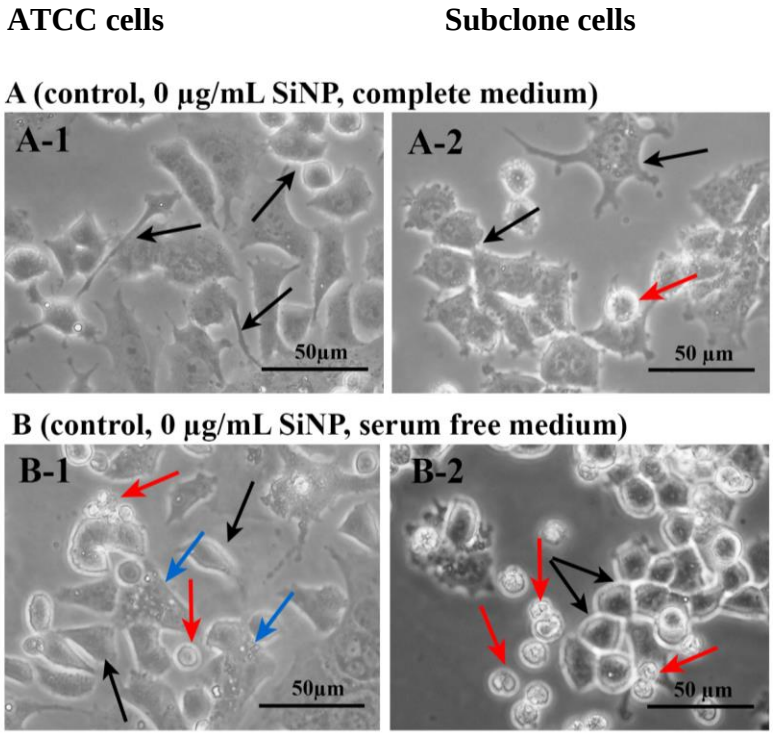

Figure 15: *Control PC12 cells grown in A) complete medium or B) serum-free medium for 24 hours. A-1, B-1: ATCC cells, A-2, B-2: subclone cells. Arrows indicate morphological characteristics. Black arrows: viable cells (neurite like structures, branching of cells and a smooth shape of the cell), red arrows: damaged cells (rounded, shrunken and fragmented), and blue arrows: vacuolization. These morphological characteristics were studied in all experiments (n > 20). Representative images.*

24 hours exposure to silica nanoparticles gave rounding and fragmentation of cells in most particle-treated groups (Fig. 16 and Fig. 17). The fraction of healthy cells seemed to be decreasing in a dose-dependent manner. Few healthy cells were observed in samples exposed to concentrations of SiNP 10 nm and 50 nm above 12.5 µg/mL (Fig. 16 and Fig. 17). A few needle-like structures and were observed in ATCC cells exposed to 25 µm/mL SiNP 50 nm (Fig. 17, D-1). The needle-like structures were not seen in either serumdeprived control, in control with complete culture medium or in silica nanoparticle-exposed subclone cells. Some vacuolization was observed in ATCC cells grown in serum-free medium (Fig. 16 B-1 and Fig. 17 C-1, E-1 E-1). Cell morphology was only studied at 24 hours of exposure because of low viability after 48 hours in serum-free exposed cells.

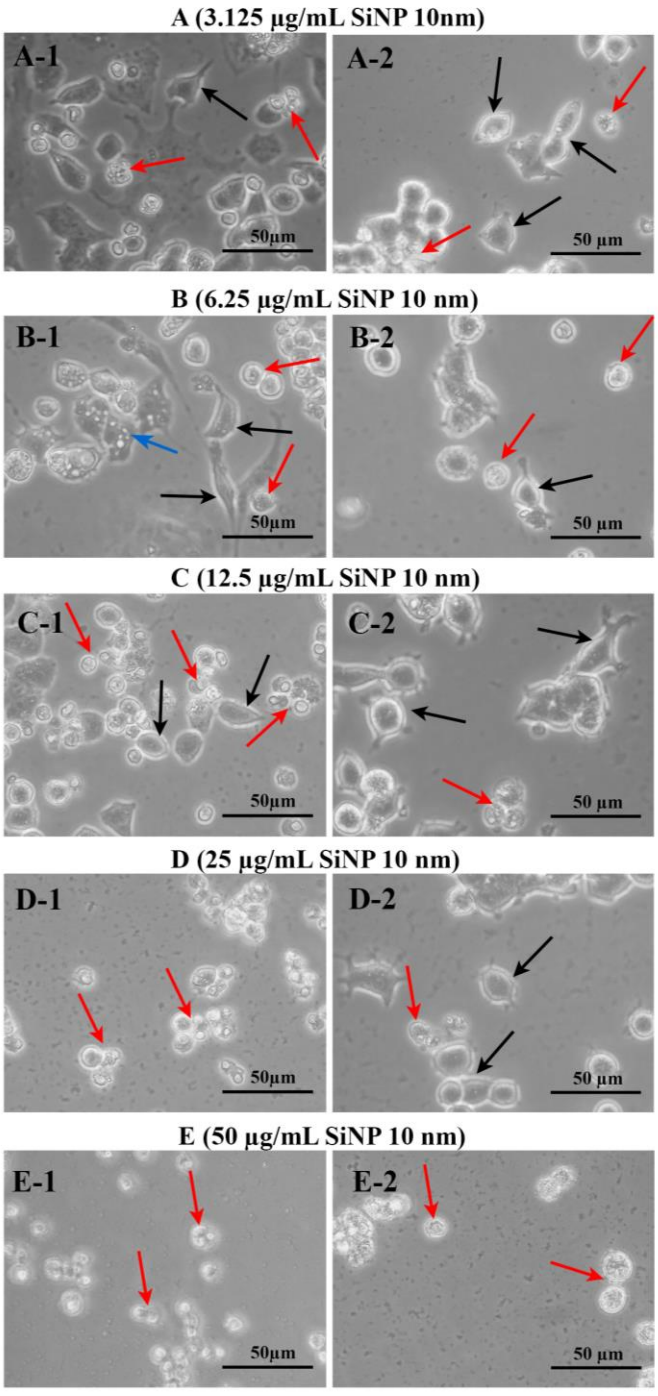

Figure 16: *PC12 cells exposed to particles (SiNP 10 nm) for 24 hours. ATCC cells (A1-E1), subclone cells (A2-E2). A1-A2: 3.125 µg/mL, B1-B2: 6.25 µg/mL, C1-C2: 12.5 µg/mL, D1-D2: 25 µg/mL, E1-E2: 50 µg/mL. Arrows indicate morphological characteristics. Black arrows: viable cells (neurite like structures, branching of cells and a smooth shape of the cell), red arrows: damaged cells (rounded, shrunken and fragmented), and blue arrows: vacuolization. These morphological characteristics were studied in all experiments (n > 20). Images are representative.*

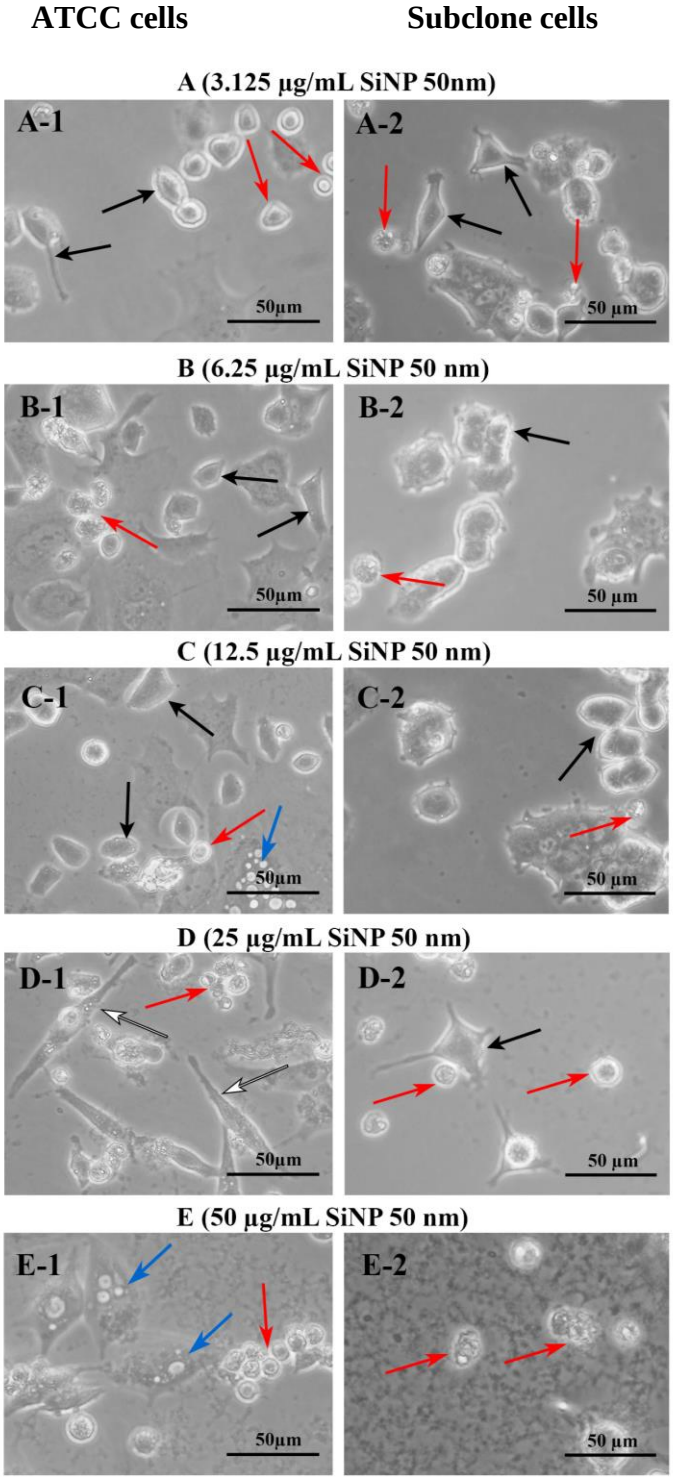

Figure 17: *PC12 cells exposed to particles (SiNP 50 nm) for 24 hours. ATCC cells (A1-E1), subclone cells (A2-E2). A1-A2: 3.125 µg/mL, B1-B2: 6.25 µg/mL, C1-C2: 12.5 µg/mL, D1-D2: 25 µg/mL, E1-E2: 50 µg/mL. Arrows indicate morphological characteristics. Black arrows: viable cells (neurite like structures, branching of cells and a smooth shape of the cell), red arrows: damaged cells (rounded, shrunken and fragmented), blue arrows: vacuolization and white arrows: needle-like structures. These morphological characteristics were studied in all experiments (n > 20). Representative images.*

4.2.2 Neurite outgrowth

A neurite outgrowth staining kit was used in attempt to quantify changes in cell surface in silica nanoparticle exposed PC12 cells, and to look for effects of SiNP on NGF-induced neurite outgrowth. As the kit failed to detect differences between NGF-treated cells (with clearly visible neurite outgrowth), and controls (without neurites), we decided not to use this kit further. Others have also abandoned this assay, due to lack of sensitivity in PC12 cells (Austdal, L. P. E, personal communication). However, the fluorescent membrane stained cells allowed us to investigate cell morphology by confocal microscopy. Subclone cells treated with NGF showed development of neurite like structures (Fig. 18). SiNP 50 nm 25µg/mL combined with serum deprivation had damaging effects in terms of rounding and fragmentation of the cells (Fig. 19). ATCC cells did not differentiate when treated with NGF.

Subclone cells

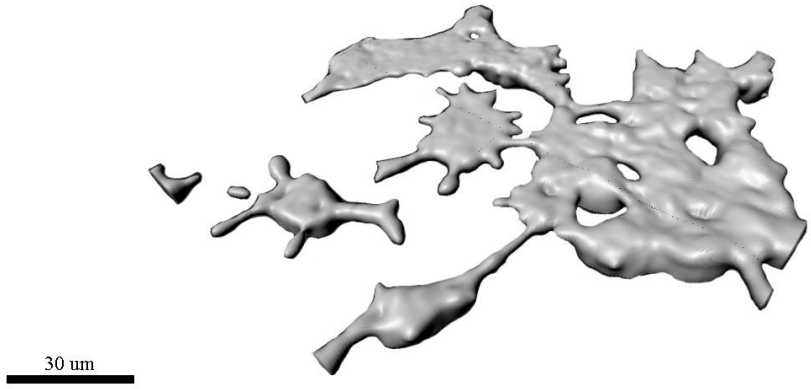

Figure 18: *Subclone cells treated with nerve growth factor in complete medium. Cells were stained with a dye from the Sigma Neurite outgrowth staining kit. Bar = 30 µm.*

Subclone cells

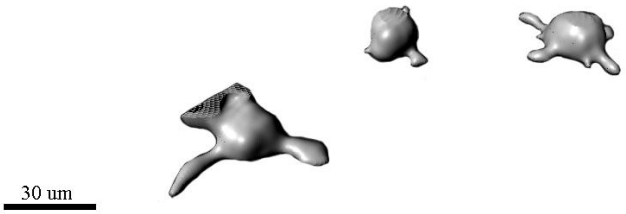

Figure 19: *Subclone PC12 cell treated with NGF in serum-free medium, exposed to 25 μg/mL SiNP 50 nm. Cells were stained with a dye from the Sigma Neurite outgrowth staining kit. Bar = 30 μm.*

4.3 Oxidative stress

4.3.1 Intracellular ROS

Results from DCF- and Rhodamine 123 fluorescence measured in ATCC cells grown in complete culture medium prior to silica nanoparticle exposure (3h) are shown in Figure 20 A-1 and B-1. Due to the high variability, only two replicates were made and no statistical analysis was done.

ATCC cells

A-1

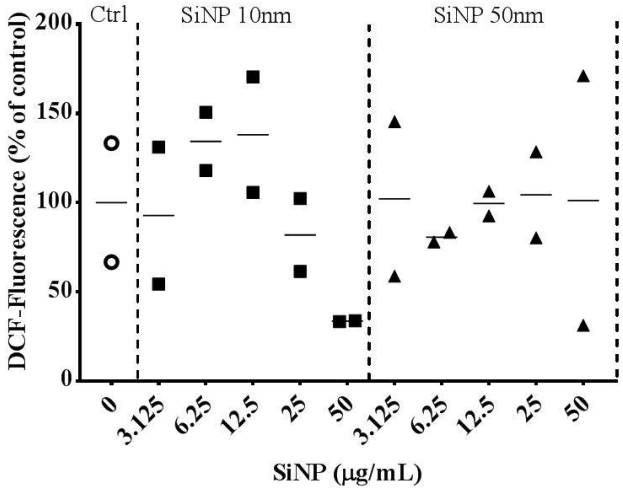

ATCC cells

B-1

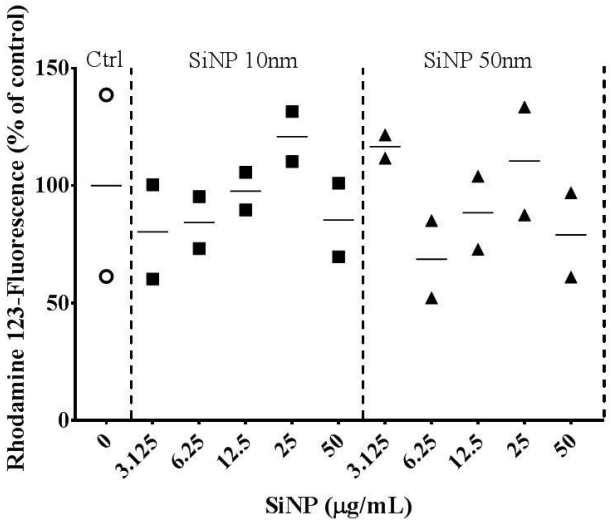

Figure 20 A-1 and B-1: *ATCC cells analyzed using a flow cytometer. Cells were grown on UpCell plates and exposed directly to silica nanoparticles (3h). A-1) Probe DCFDA measuring the fluorescent compound DCF, B-1) Probe DHR, measuring the fluorescent compound Rhodamine 123. Normalized to serum free control (0). No statistical analysis was done (n=2).*

Cells serum deprived for 24 hours prior to exposure

In an attempt to reduce variability, cells were grown in serum-free medium 24 hour prior to exposure. This was done in both ATCC and sub clone cells (Fig. 21). Results are shown in Figure 8. No significant linear trend was found using multiple comparison tests in any of the three experiments.

In general, ATCC cells stained with DCFDA probe had low fluorescent activity (Fig. 21 A-1). ATCC cells with DHR probe showed an increase in fluorescence at concentrations higher than 3.125 µg/mL 10 nm SiNP (Fig. 21 B-1). A decrease was seen in the same experiment with concentrations higher than 12.5 µg/ml 50 nm SiNP.

In subclone cells DCF-fluorescence seemed to increase with increasing concentration of silica nanoparticles of both sizes, although not significant (Fig. 21 A-2). SiNP 50 nm exposed subclone cells had lower levels of measured fluorescent DCF than cells exposed to SiNP 10 nm.

ATCC cells

A-1

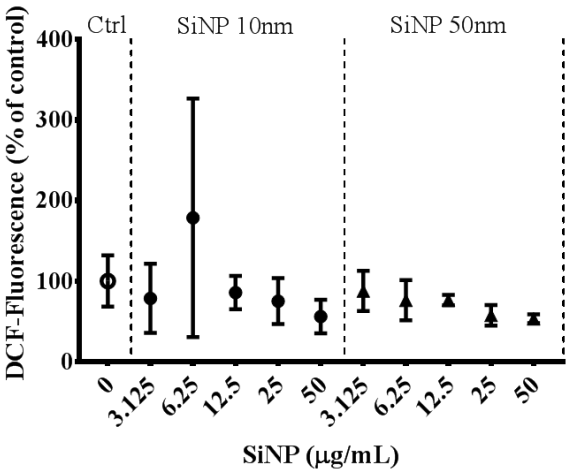

Subclone cells

A-2

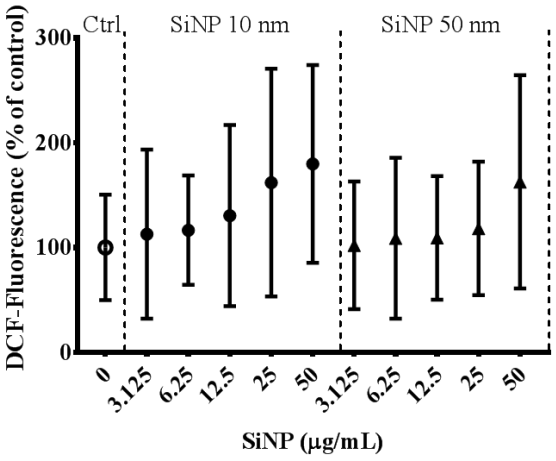

ATCC cells

B-1

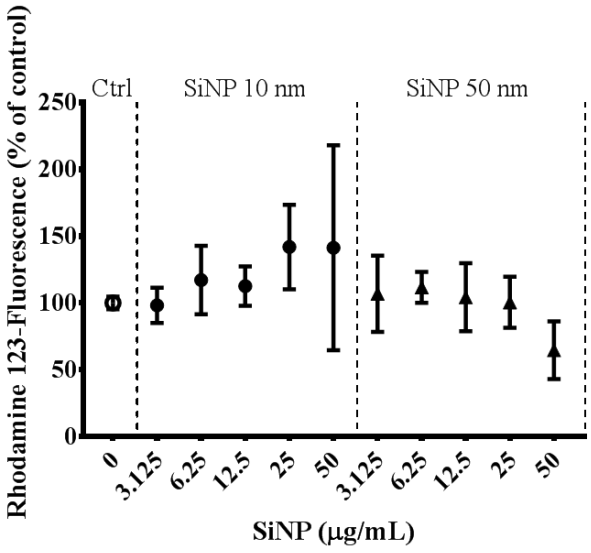

Figure 21 A-1, B-1 and B-2: *Fluorescence measured after 3 hours of SiNP exposure, 24 hours in serum free medium. Normalized to serum free control (0). A-1 and B-1) ATCC cells, flow cytometer, B-2) subclone cells, plate reader. A significant linear trend was found in A-1 ($p=0.00064$ in SiNP 10 nm). All statistical analysis is performed by One-way ANOVA, Dunnett's multiple comparison test and test for linear trend between column mean and left to right column order ($p \leq 0.05$ is considered statistically significant). The results are shown as mean ± SD (n=3).*

4.3.2 Western blot

Western blot was used to determine the level of heme oxygenase-1. α-Tubulin was used as loading control. HO-1 levels in positive control with HEMA (2 mM) were significantly higher when compared to serum-free control (Appendix 10). Cells grown in complete medium (control) was not significantly different from cells grown in serum-free control (Appendix 10). No significant difference from serum-free control was found at any concentration of SiNP 10 nm or SiNP 50 nm (Fig. 22). The standard deviation is large in SiNP 10 nm exposed cells, but the median is generally lower than the serum-free control. Cells exposed to SiNP 50 nm have even lower levels of relative heme oxygenase-1.

Subclone cells

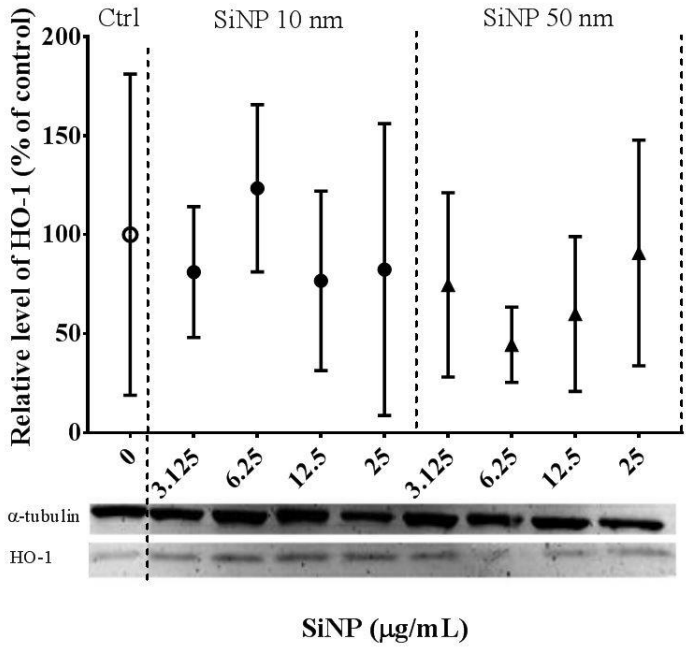

Figure 22: *Relative level of HO-1 after 24 hours of SiNP exposure, normalized to serum free control (0). B-1) ATCC cells, B-2) subclone cells. One-way ANOVA was significant ($p<0.0001$, $F=26.25$). All statistical analysis is performed by One-way ANOVA, Dunnett's multiple comparison test and test for linear trend between column mean and left to right column order ($p \leq 0.05$ is considered statistically significant). The results are shown as mean ± SD (n=4). Blots: α-Tubulin (loading control), HO-1 (biomarker enzyme).*

5 Discussion

Nano-sized silica particles are used in numerous biomedical applications due to their many physicochemical properties (Wang et al., 2011; Wu et al., 2011). Dental treatment with resin-based composites is one of the most frequent uses of such materials. However, the requirements for toxicity testing of dental restoratives are limited. Hence, knowledge regarding toxicity of nanoparticles released from dental materials is insufficient. Although silica nanoparticle toxicity has been studied in many *in vitro* studies, most of these are designed from an airway exposure perspective (Asweto et al., 2017; Khalili et al., 2015; Låg et al., 2018). Considering the size of these particles, they are thought to be able to cross the blood-brain barrier where they can interfere with neurons (Wu et al., 2011). It is therefore pertinent to study the possible neurotoxic effects of such particles. In this study, neurotoxicity induced by silica nanoparticles used in dental materials was studied in PC12 cells. Effects of these nanoparticles were studied using several well-established methods such as changes in cell morphology (phase contrast microscopy, confocal microscopy), oxidative stress (release of ROS and level of heme-oxygenase proteins), cell viability (MTT), and cell death (HOECHST 33342/PI staining).

5.1.1 Decreased cell viability and increased cell death

A dose-dependent reduction in cell viability was seen in ATCC cells exposed to SiNP 10 and 50 nm for 24 and 48 hours, as measured by the MTT-assay. Despite the large variation in subclone cells and the lack of significant differences using the Dunnett's multiple comparison test, the one-way ANOVA analysis provided significant reduced viability after 48 hours exposure. No significant results in 24 hours exposed subclone cells could be due to the high variation in the experiments. This could indicate that this clone contains a more heterogeneous cell population. The linear trend was significant in SiNP 10 nm exposed cells, suggesting a dose-response. A higher cell viability in SiNP 50 nm exposed cells is in line with our hypothesis, that smaller particles are more damaging to the cells than the larger ones. This is also in agreement with previous studies by Wang and colleagues (2011). A possible explanation is the smaller particles' ability to cross cell membranes more easily.

In subclone cells, a higher toxic potential of SiNP 10 nm compared to SiNP 50 nm is also indicated by the measurement of apoptotic and necrotic cell death after 24 hours exposure. However, only one experiment was carried out, and further experiments are needed to verify

this result. A high proportion of necrotic cells were seen after 48 hours. Since this effect is seen in both control cells and exposed cells, it is likely to assume that serum deprivation is the main cause for this effect. In line with this, earlier studies have suggested that serum deprivation induces cell death and reduces cell viability in PC12 cells (Greene & Tischler, 1976; Rakkestad et al., 2014).

5.1.2 Silica nanoparticles induces morphological changes in PC12 cells

Phase contrast microscopy images showed fragmentation, shrinkage and rounding in most SiNP exposed ATCC and sub clone PC12 cells. This could indicate apoptotic cells, as cell shrinkage is a common hallmark of this process. Cells with these characteristics were abundant in silica nanoparticle exposed cells, especially those exposed to higher concentrations of SiNP 10 nm. These results were based on visual characterization and did not provide data suitable for statistical analysis, but this could possibly correlate well with our data on apoptotic measurements. Less shrinkage and fragmentation was observed in SiNP 50 nm treated cells, compared to SiNP 10 nm. This gives us reason to assume that the apoptotic rate is lower in these cells. These findings are in line with our measurements of cell viability that suggest a size-dependent toxicity of silica nanoparticles on PC12 cells.

Vacuolization was observed in ATCC cells treated with SiNP. This is also found in earlier studies (Larner et al., 2017), suggesting that different types of nano-sized particles induces cytosolic vacuoles in PC12 cells. Wang and colleagues (Wang et al., 2011) showed that SiNPs entered the cell. One could speculate that the observed vacuoles are lysosomes increasing in size due to particle uptake. Lysosome impairment in cells exposed to silica nanoparticle has previously been reported (Ma et al., 2011; Schütz et al., 2016). Schütz and co workers reported that internalized SiNPs accumulate in the lysosomes, thereby inducing cell death. Vacuolization was not observed in subclone cells, neither decreased cell viability after 24 hours exposure. This could indicate that the observed differences in ATCC and subclone cell viability after SiNP exposure is due to particle uptake. This hypothesis, however, needs to be verified by other more specific methods such as scanning electron microscopy. The observed difference in cellular uptake between the tested cell clones does *not* support a passive particle uptake mechanism as previously suggested (Shen et al., 2018; Song et al., 2017).

Needle-like structures were seen in ATCC cells exposed for 24 hours to 25 μm/mL SiNP 50 nm. In a similar study where the same subclone cells were used (Farajalla, 2015), these structures were observed 72 hour after exposure, but not after 24 hours or 48 hours. This indicates that this phenotype need more time to develop in the subclone cells. Further characterization of both the mechanisms of development and the functions of these structures is needed to better understand this difference between the cell clones.

A quantification of the morphological changes observed would have been possible, e.g. by counting cells with different structures, but such procedures are time consuming, and the results often depend on the operator and can be difficult to reproduce. A quick and objective procedure to quantify morphological changes would therefore have been desirable. In this study, a neurite outgrowth kit was tested for this purpose. Unfortunately, the use of this kit was showed to be difficult, and did not provide any meaningful results. Visual observation by confocal laser scanning microscopy was done on fluorescently stained cells, and supported our findings of rounding and fragmentation of silica nanoparticle exposed cells.

5.1.3 The effect of silica nanoparticles on ROS levels and oxidative stress

Increased reactive oxidative stress has been suggested as an important event during particle induced cell death (Fu et al., 2014). After 3 hour of exposure, our experiments could not find any significant increase ROS. This result, however, does not exclude the possibility that increased levels of ROS are an important event in the onset of cell death. The underlying mechanism of ROS increase is an important factor that determines when the ROS increase is measurable. In 2,2′-azobis (amidinopropane) dihydrochloride exposed PC12 cells, the ROS levels reached the max level after 1 hour and decreased thereafter (Piga, Saito, Yoshida, & Niki, 2007). Wang and colleagues reported a dose-dependent ROS increase in PC12 cells exposed to SiNPs for 24 hours (Wang et al., 2011). To investigate if ROS precede the cell death we chose to measure ROS after 3 hours, considering the cell viability reduction that was evident after 24 hours of exposure. Since a ROS increase may be limited to a narrow time window (Piga et al., 2007), more time points must be investigated before excluding ROS formation as an important event in nanoparticle induced PC12 toxicity.

As mentioned as an explanation for the variation in cell viability in subclone cells, a more heterogeneous cell population could also be a possible explanation for the large standard

deviation found in our ROS data. It is also possible that ROS increases to toxic levels in local compartments of the PC12 cells exposed to SiNPs for 3 hours without affecting the total ROS level of the cells to a clearly measurable extent. In the subclone cells, the measured mean ROS levels increased slightly, although not significant, with increasing nanoparticle concentration. Keeping in mind that these cells were treated with serum deprivation 24 hours prior to exposure, there is a possibility that nanoparticles enhance an effect of this serum deprivation, or that cells produce more ROS when cultured in serum-free medium as shown in earlier studies (Satoh, Sakai, Enokido, Uchiyama, & Hatanaka, 1996). Another possible side effect of the serum deprivation is that cells are more easily detached from the growth surface. This could skew the number of measured cells, as the serumdeprived will be more numerous. Hence, changes in ROS levels being an important event in response to nanoparticle-induced stress cannot be verified or excluded from these measurements. However, after 24 hours there was no significant increase in HO-1 levels in silica nanoparticle exposed cells as would have been expected as a response to oxidative stress (Kikuchi, Yoshida, & Noguchi, 2005). The amount of protein in the western blotting samples was evaluated based on Ponceau S staining and by relating heme oxygenase 1 to a loading control (alpha tubulin). We assume that α-Tubulin is equally expressed in all the samples. By dividing the values of α-Tubulin from the HO-1 values we can ensure that the amount of proteins in the samples were the same. This method offers some difficulties as the calculations done on these data are not linear, and therefor less precise. However, the significant HO-1 level after exposure to HEMA (positive control) shows that the method detects altered HO-1 levels.

The consistent differing results between the two probes indicate production of various oxygen species in the cells, suggests a higher abundance of peroxide, peroxynitrite, or superoxide than hydroxyl and peroxyl in ATCC cells (Wang et al., 2011).

5.1.4 ATCC and subclone cells gives different results

Two cell clones with the same origin and thought to have the same characteristics, were studied. The exposed ATCC cells demonstrated cellular vacuolization, needle-like structures, significantly reduced viability after exposure, and were more adherent. The subclone cells differentiated in response to NGF by developing neurite like structures, but showed high variation, possibly due to heterogeneity. The large variety in our results underlines the

uncertainties associated with conclusions drawn from studies based on one cell clone. Heterogeneous cell cultures could give a selection for the fastest growing cells, and studies have also shown that differences in passage number may give false-positive/false-negative results (Kinarivala, Shah, Abbruscato, & Trippier, 2017).

5.1.5 Nanoparticles in dentistry

The combination of cell viability measurements, morphology studies and characterization of oxidative stress could indicate that SiNP exposure has negative effects on neurons. Therefore, care should be taken to minimize exposure on dental personnel and patients. However, although the PC12 cell line offers neuron like features, they are not actual neurons. The lack of complexity such as essential synapse connections found in real neurons is not available. Thus the results cannot be directly transferred to real neurons in the human brain, which is important to be aware of when evaluating the results in a broader perspective. A more wide-ranging study is needed to investigate these findings further (de los Rios et al., 2017; Greene & Tischler, 1976; Radio & Mundy, 2008). Also, it is important to keep in mind that the concentrations used in vitro are usually higher than what we are exposed to in real life. Moreover, the exposures done in our studies are brief, and far from the real life exposure of dental personnel that could be exposed several hours a day and throughout their whole career.

6 Conclusions

Based on the results from this thesis, I conclude that silica nanoparticles affects several biological processes in PC12 cells that could alter the function and structure of neurons:

- Cell viability was dose-dependently decreasing in silica nanoparticle exposed cells
- The NGF response was found to be cell batch dependent
- In this this study there was no data clearly indicating ongoing oxidative stress, as increased ROS and HO-1 was not found
- The ATCC cells and subclone cells differs and responds differently to parallel exposure. This shows the importance of including several cell clones in a study
- Silica nanoparticles seem to have different toxicity based on their size

7 Future perspectives

In this study we demonstrated that silica nanoparticles reduces cell viability in a dose-dependent matter. However the data on mechanisms behind reduced cell viability remains to be fully investigated. It would be of interest to run several experiments of cell death classification and ROS. More data would provide valuable measures to run statistical tests supporting our findings.

Effects of silica nanoparticles on cell morphology was investigated and for future studies, quantify the number and surface area of neurites per cell would be interesting.

Using the western blotting analysis it would be of interest to investigate the effect of antioxidants on exposed cells as well as other biomarker molecules for stress responses in cells.

References

Anderson, J. M., & Van Itallie, C. M. (2009). Physiology and Function of the Tight Junction. *Cold Spring Harbor Perspectives in Biology, 1*(2), a002584.

Anusavice, K. J., Phillips, R. W., Shen, C., & Rawls, H. R. (2013). *Phillips' Science of Dental Materials*: Elsevier/Saunders.

Aprioku, J. S. (2013). Pharmacology of Free Radicals and the Impact of Reactive Oxygen Species on the Testis. *Journal of Reproduction & Infertility, 14*(4), 158-172.

Asweto, C. O., Wu, J., Alzain, M. A., Hu, H., Andrea, S., Feng, L., et al. (2017). Cellular pathways involved in silica nanoparticles induced apoptosis: A systematic review of in vitro studies. *Environmental Toxicology and Pharmacology, 56*, 191-197.

Brodal, P. (2013). *Sentralnervesystemet* (5 ed.). Oslo: Universitetsforlaget.

Calabrese, V., Mancuso, C., De Marco, C., Stella, A. M. G., & Butterfield, D. A. (2007). Nitric Oxide and Cellular Stress Response in Brain Aging and Neurodegenerative Disorders. In S. H. Parvez & G. A. Quresh (Eds.), *Oxidative Stress and Neurodegenerative Disorders* (pp. 115-134). Amsterdam: Elsevier Science B.V.

Cummings Brian, S., & Schnellmann Rick, G. (2004). Measurement of Cell Death in Mammalian Cells. *Current Protocols in Pharmacology, 25*(1), 12.18.11-12.18.22.

de los Rios, C., Cano-Abad, M. F., Villarroya, M., & López, M. G. (2017). Chromaffin cells as a model to evaluate mechanisms of cell death and neuroprotective compounds. *Pflügers Archiv - European Journal of Physiology, 470*(1), 187-198.

Eom, H.-J., & Choi, J. (2009). Oxidative stress of silica nanoparticles in human bronchial epithelial cell, Beas-2B. *Toxicology in Vitro, 23*(7), 1326-1332.

European Commission. (2016, 22.02.2017). Definition of a nanomaterial. Retrieved from http://ec.europa.eu/environment/chemicals/nanotech/faq/definition_en.htm

Fan, Z., Fu, P. P., Yu, H., & Ray, P. C. (2014). Theranostic nanomedicine for cancer detection and treatment. *Journal of Food and Drug Analysis, 22*(1), 3-17.

Farajalla, T. (2015). *Silika nanopartikler endrer morfologi og øker glutamat cystein ligase promotoraktiviteten i PC12-celler*. (Masters thesis), University of Oslo.

Feng, X., Chen, A., Zhang, Y., Wang, J., Shao, L., & Wei, L. (2015). Application of dental nanomaterials: potential toxicity to the central nervous system. *International Journal of Nanomedicine, 10*, 3547-3565.

Fu, P. P. (2014). Introduction to the Special Issue: Nanomaterials— Toxicology and medical applications. *Journal of Food and Drug Analysis, 22*(1), 1-2.

Fu, P. P., Xia, Q., Hwang, H.-M., Ray, P. C., & Yu, H. (2014). Mechanisms of nanotoxicity: Generation of reactive oxygen species. *Journal of Food and Drug Analysis, 22*(1), 64-75.

Fujita, K., Lazarovici, P., & Guroff, G. (1989). Regulation of the differentiation of PC12 pheochromocytoma cells. *Environmental Health Perspectives, 80*, 127-142.

Greene, L. A., & Tischler, A. S. (1976). Establishment of a noradrenergic clonal line of rat adrenal pheochromocytoma cells which respond to nerve growth factor. *Proceedings of the National Academy of Sciences of the United States of America, 73*(7), 2424-2428.

Hancock, J. T., Desikan, R., & Neill, S. J. (2001). Role of reactive oxygen species in cell signalling pathways. *Biochemical Society Transactions, 29*(2), 345.

He, W., Liu, Y., Wamer, W. G., & Yin, J.-J. (2014). Electron spin resonance spectroscopy for the study of nanomaterial-mediated generation of reactive oxygen species. *Journal of Food and Drug Analysis, 22*(1), 49-63.

He, X., Aker, W. G., Leszczynski, J., & Hwang, H.-M. (2014). Using a holistic approach to assess the impact of engineered nanomaterials inducing toxicity in aquatic systems. *Journal of Food and Drug Analysis, 22*(1), 128-146.

Hennigan, A., Callaghan, R. M., & Kelly, Á. M. (2007). Neurotrophins and their receptors: roles in plasticity, neurodegeneration and neuroprotection. *Biochemical Society Transactions, 35*(2), 424.

Hildebrand Hartmut, F. (2013). Biomaterials – a history of 7000 years. *BioNanoMaterials, 14*(3-4), 119.

Hotchkiss, R. S., Strasser, A., McDunn, J. E., & Swanson, P. E. (2009). Cell Death. *New England Journal of Medicine, 361*(16), 1570-1583.

Huang, E. J., & Reichardt, L. F. (2001). Neurotrophins: Roles in Neuronal Development and Function. *Annual review of neuroscience, 24*, 677-736.

Karmakar, A., Zhang, Q., & Zhang, Y. (2014). Neurotoxicity of nanoscale materials. *Journal of Food and Drug Analysis, 22*(1), 147-160.

Kerr, J. F. R., Wyllie, A. H., & Currie, A. R. (1972). Apoptosis: A Basic Biological Phenomenon with Wide-ranging Implications in Tissue Kinetics. *British Journal of Cancer, 26*(4), 239-257.

Khalili, J. F., Jafari, S., & Eghbal, M. A. (2015). A Review of Molecular Mechanisms Involved in Toxicity of Nanoparticles. *Advanced Pharmaceutical Bulletin, 5*(4), 447-454.

Kikuchi, G., Yoshida, T., & Noguchi, M. (2005). Heme oxygenase and heme degradation. *Biochemical and Biophysical Research Communications, 338*(1), 558-567.

Kinarivala, N., Shah, K., Abbruscato, T. J., & Trippier, P. C. (2017). Passage Variation of PC12 Cells Results in Inconsistent Susceptibility to Externally Induced Apoptosis. *ACS Chemical Neuroscience, 8*(1), 82-88.

Krifka, S., Hiller, K.-A., Spagnuolo, G., Jewett, A., Schmalz, G., & Schweikl, H. (2012). The influence of glutathione on redox regulation by antioxidant proteins and apoptosis in macrophages exposed to 2-hydroxyethyl methacrylate (HEMA). *Biomaterials, 33*(21), 5177-5186.

Lai, T.-H. S., Jiunn-Min; Tsou, Chih-Jen; Wu, Wen-Bin. (2015). Gold nanoparticles induce heme oxygenase-1 expression through Nrf2 activation and Bach1 export in human vascular endothelial cells. *International Journal of Nanomedicine, 10*, 5925-5939.

Larner, S. F., Wang, J., Goodman, J., O'Donoghue Altman, M. B., Xin, M., & Wang, K. K. W. (2017). In Vitro Neurotoxicity Resulting from Exposure of Cultured Neural Cells to Several Types of Nanoparticles. *Journal of Cell Death, 10*.

Levi-Montalcini, R., Skaper, S. D., Dal Toso, R., Petrelli, L., & Leon, A. (1996). Nerve growth factor: from neurotrophin to neurokine. *Trends in Neurosciences, 19*(11), 514-520.

Låg, M., Skuland, T., Godymchuk, A., Nguyen, T. H. T., Pham, H. L. T., & Refsnes, M. (2018). Silica Nanoparticle-induced Cytokine Responses in BEAS-2B and HBEC3-KT Cells: Significance of Particle Size and Signalling Pathways in Different Lung Cell Cultures. *Basic & Clinical Pharmacology & Toxicology, 122*(6), 620-632.

Ma, X., Wu, Y., Jin, S., Tian, Y., Zhang, X., Zhao, Y., et al. (2011). Gold Nanoparticles Induce Autophagosome Accumulation through Size-Dependent Nanoparticle Uptake and Lysosome Impairment. *ACS Nano, 5*(11), 8629-8639.

Mahmood, T., & Yang, P.-C. (2012). Western blot: Technique, theory, and trouble shooting. *North American Journal of Medical Sciences, 4*(9), 429-434.

Majno, G., & Joris, I. (1995). Apoptosis, oncosis, and necrosis. An overview of cell death. *The American Journal of Pathology, 146*(1), 3-15.

Migliore, L., Uboldi, C., Di Bucchianico, S., & Coppedè, F. (2015). Nanomaterials and neurodegeneration. *Environmental and Molecular Mutagenesis, 56*(2), 149-170.

Mirshafa, A., Nazari, M., Jahani, D., & Shaki, F. (2017). Size-Dependent Neurotoxicity of Aluminum Oxide Particles: a Comparison Between Nano- and Micrometer Size on the Basis of Mitochondrial Oxidative Damage. *Biological Trace Element Research, 183*(2), 261-269.

Murugadoss, S., Lison, D., Godderis, L., Van Den Brule, S., Mast, J., Brassinne, F., et al. (2017). Toxicology of silica nanoparticles: an update. *Archives of Toxicology, 91*(9), 2967-3010.

Oh, N., & Park, J.-H. (2014). Endocytosis and exocytosis of nanoparticles in mammalian cells. *International Journal of Nanomedicine, 9*(1), 51-63.

Peixoto, M. S., de Oliveira Galvão, M. F., & Batistuzzo de Medeiros, S. R. (2017). Cell death pathways of particulate matter toxicity. *Chemosphere, 188*, 32-48.

Piga, R., Saito, Y., Yoshida, Y., & Niki, E. (2007). Cytotoxic effects of various stressors on PC12 cells: Involvement of oxidative stress and effect of antioxidants. *NeuroToxicology, 28*(1), 67-75.

Radio, N. M., & Mundy, W. R. (2008). Developmental neurotoxicity testing in vitro: Models for assessing chemical effects on neurite outgrowth. *NeuroToxicology, 29*(3), 361-376.

Rakkestad, K. E., Sørvik, I. B., Øverby, G. R., Debernard, K. A. B., Mathisen, G. H., & Paulsen, R. E. (2014). 17α-Estradiol down-regulates glutathione synthesis in serum deprived PC-12 cells. *Free Radical Research, 48*(10), 1170-1178.

Satoh, T., Sakai, N., Enokido, Y., Uchiyama, Y., & Hatanaka, H. (1996). Survival factor-insensitive generation of reactive oxygen species induced by serum deprivation in neuronal cells. *Brain Research, 733*(1), 9-14.

Schmalz, G., & Arenholt-Bindslev, D. (2009). *Biocompatibility of Dental Materials*. Berlin, Germany: Springer

Schütz, I., Lopez-Hernandez, T., Gao, Q., Puchkov, D., Jabs, S., Nordmeyer, D., et al. (2016). Lysosomal Dysfunction Caused by Cellular Accumulation of Silica Nanoparticles. *The Journal of Biological Chemistry, 291*(27), 14170-14184.

Shen, Y., Cao, B., Snyder, N. R., Woeppel, K. M., Eles, J. R., & Cui, X. T. (2018). ROS responsive resveratrol delivery from LDLR peptide conjugated PLA-coated mesoporous silica nanoparticles across the blood–brain barrier. *Journal of Nanobiotechnology, 16*(1), 13.

Song, Y., Du, D., Li, L., Xu, J., Dutta, P., & Lin, Y. (2017). In Vitro Study of Receptor-Mediated Silica Nanoparticles Delivery across Blood-Brain Barrier. *ACS applied materials & interfaces, 9*(24), 20410-20416.

Sun, L., Li, Y., Liu, X., Jin, M., Zhang, L., Du, Z., et al. (2011). Cytotoxicity and mitochondrial damage caused by silica nanoparticles. *Toxicology in Vitro, 25*(8), 1619-1629.

Tang, L., & Cheng, J. (2013). Nonporous Silica Nanoparticles for Nanomedicine Application. *Nano today, 8*(3), 290-312.

Van Landuyt, K. L., Yoshihara, K., Geebelen, B., Peumans, M., Godderis, L., Hoet, P., et al. Should we be concerned about composite (nano-)dust? *Dental Materials, 28*(11), 1162-1170.

Vincent, A. M., Russell, J. W., Low, P., & Feldman, E. L. (2004). Oxidative Stress in the Pathogenesis of Diabetic Neuropathy. *Endocrine Reviews, 25*(4), 612–628.

Wang, F., Jiao, C., Liu, J., Yuan, H., Lan, M., & Gao, F. (2011). Oxidative mechanisms contribute to nanosize silican dioxide-induced developmental neurotoxicity in PC12 cells. *Toxicology in Vitro, 25*(8), 1548-1556.

Williams, D. F. (1987). Tissue-biomaterial interactions. *Journal of Materials Science*, *22*(10), 3421-3445.

Wu, J., Wang, C., Sun, J., & Xue, Y. (2011). Neurotoxicity of Silica Nanoparticles: Brain Localization and Dopaminergic Neurons Damage Pathways. *ACS Nano, 5*(6), 4476-4489.

Yamaguchi, Y., & Miura, M. (2015). Programmed Cell Death in Neurodevelopment. *Developmental Cell, 32*(4), 478-490.

Zhu, C.-L., Wang, X.-W., Lin, Z.-Z., Xie, Z.-H., & Wang, X.-R. (2014). Cell microenvironment stimuli-responsive controlled-release delivery systems based on mesoporous silica nanoparticles. *Journal of Food and Drug Analysis, 22*(1), 18-28.

Appendix

Appendix 1 Cell culturing

Table 6: *Cell clones used in this thesis*

Cell type	Description	Supplier
PC12 Adh (ATCC® CRL-1721.1™)	*Rattus norvegicus*, rat cell line: Polygonal cells collected from adrenal gland.	ATCC
PC12 subclone	*Rattus norvegicus*, rat cell line: Polygonal cells collected from adrenal gland.	Kindly given from Ragnhild Paulsen's laboratory at Department of Pharmacy, UiO

Appendix 2 Cell exposure

Preparation of nanoparticle solution

1. Micro tubes with SiNP10 and SiNP50 was vortexed 1 min.
2. 1 mL SiNP 10nm (2,3 mg/μL) and 1 mL SiNP 50nm (2,3 mg/μL) was added to two separate eppendorf tubes with screw cap.
3. Each tube was sonicated at the following settings:
   50 % amplitude
   3 x cycles
   180 Joule
4. 34,5 μL BSA (in dH_2O 50mg/mL) and 115 μL PBS was added to each tube after sonication and vortexed 1 min.
5. Nanoparticle solution was mixed with serum-free medium in varying concentrations: 3.125 μg/mL, 6.25 μg/mL, 12.5 μg/mL, 25 μg/mL and 50μg/mL (SiNP 10 nm and SiNP 50 nm).

Nanoparticle exposure

1. Cells were exposed after 24h incubation at a stable 5% CO_2 and 37° C.
2. Old medium was removed.
3. 500 μL PBS was carefully added to each well.
4. PBS was carefully removed.

5. NP solution was added to the wells.
6. Cells were incubated for 3h, 24h or 48h at 5% CO_2 and 37° C before further analysis were done.

Appendix 3 MTT-assay

1. After 24h incubation, medium was removed
2. 400 μL MTT-regent per well in a 24-well plate were added and incubated at 37°C, 5% CO_2.
3. MTT-regent was removed and 400 μL DMSO was added to each well
4. Plate were shaken 10-15 minutes until the formazan crystals was dissolved
5. 200 μL of the dissolved solution from each well at the 24-well plate was transferred to 24 wells in a 96-well plate
6. Samples were analyzed in a multiwall scanning spectrophotometer.

MTT-stock solution consists of 1 mL MTT, 9 mL PBS.

Appendix 4 Cell death classification

1. After incubating and exposing samples, old medium was removed and added to a new eppendorf tube
2. 200μL Trypsin was added to each cell dish, then added to the eppendorf tube together with the medium. Repeated twice
3. 100μL Trypsin was added to each cell dish and was incubated in CO_2-incubator 3-10 min. When cells were loose, the samples were added to the eppendorf tubes
4. Eppendorf tubes were centrifuged (10 min, 250g)
5. Supernatant was kept
6. Serum with HOECHST 33342/PI was added and incubated for 30 min at room temperature, protected from light
7. One drop is pipetted onto a microscope slide and spread out using a clean microscope slide
8. Slides were dried in room temperature and protected against light before studied in a florescence microscope (filter 4, 100x magnitude with oil)
9. 300 cells was counted from each sample

Appendix 5 Phase contrast microscopy

Cells were analyzed at 10x and 20x magnification in Olympus CKX41 Inverted Phase Contrast Microscope. Pictures were taken at 20x magnification using Olympus Camedia C-7070 camera. A Bürker chamber was used to make a correct scaling of the pictures in Adobe Photoshop CS6.

Appendix 6 Neurite outgrowth staining kit

96-well cell culture plates were used, adding 100 μL solution to each well with 4000 cells/well (40 000 cells/mL). Cells were counted and average size measured to calculate the ratio between cell suspension and medium. A multi pipette was used to add 100μL cell suspension to each well before incubation at 37°C, 5% CO_2 for 24 hours.

The following day, Nerve growth factor (NGF) solution was prepared:

1. NGF, 10μg/mL (diluted in serum-free medium). Need 1000μg/mL (1:100). 40μg NGF-solution was added to 4 medium and vortexed 1 minute.
2. Nanoparticle solutions were made as described in 2.1.4
3. Old medium was removed carefully and 100μL PBS was added. PBS was removed by tilting the 96-well plate up side down in an autoclave bag.
4. Cells were exposed one well at the time to avoid the cells to dry out.
5. Cells were incubated at 37°C, 5% CO_2 for 24 hours.
6. Light microscopy was used to look for morphological changes, and pictures were taken for later comparison.
7. Cells were incubated at 37°C, 5% CO_2 for 24 hours again.
8. Light microscopy was used to look for morphological changes, and pictures were taken for later comparison.
9. Old medium was carefully removed and new complete medium was added.
10. 10 μL cell viability indicator, 10 μL 1x cell membrane stain and 10 μL DPBS buffer was mixed
11. 100 μL of the working stain solution (10.) was added to each well. Incubate 10-20 min
12. 1 x cell membrane was removed
13. 100 μL 1x working solution background suppression stain (10 mL DPBS and 100 μL background stain) was added to each well (Table 7).
14. Analysis was done in fluorescent plate reader.

1 x working stain solution (WSS),

1 x working solution background suppression stain (WSBSS),

1 x working/fix stain solution (WFSS),

1 x working solution background suppression dye (SBSD)

Table 7: *Preparation of NGF staining solution*

Constituent	**WSS**	**WSBSS**	**WFSS**	**SBSD**
Buffer (DPBS)	10 mL	10 mL		10 mL
Cell viability indicator	10 μL		10 μL	
Cell membrane stain	10 μL		10 μL	
Background stain		100 μL		100 μL
PFA 3.9 % in PBS			10 mL	

Appendix 7 ROS-measurements

Cells were grown on 2x12 well cell plates for 24 hours before exposure. Cell density was 40 000 cells/mL, and 1 mL cell suspension with nanoparticle solution was added to each well after removing old medium with serum and washing with PBS. Cells were exposed for 3 hours, before collecting and analyzing the samples.

Preparation of probe solutions

1. Probes used were H2-DCFDA and DHR. 29μL DMSO was added to the bottle of DCFDA, then 15μL of this solution was mixed with 135μL serum-free medium. The DHR probe was mixed with 135μL serum-free medium. 8μL of the DCFDA solution was added to each well on one of the plates, and 10μL of the DHR solution was added to each well on the other plate.
2. Samples were incubated for 15 minutes at 37°C and 5% CO_2.
3. 500μL PBS/FBS solution was added to each well on both plates after removing old solution from the samples. PBS/FBS solution consists of 140μL Fetal Bovine Serum (FBS) and 14μL PBS mixed together.

4. Using Thermo Scientific Nuc UpCell surface plates, incubation time were 30 minutes in room temperature or until cells were loose. Non-coated plates did not require incubation time and was collected immediately.
5. Samples were kept dark and on ice. Analyzing the samples were done using a Flow Cytometer.

Appendix 8 Western blot

1. The cube was mounted and the samples were defrosted.
2. Prepared separating gel according to table 9. The first four components were mixed carefully, then the two latter below the stippled line. When the APS and TEMED are added, the gel starts to set. 7 mL of the gel were added between the glass plates. Last, distilled water was added on top of the gel in the cube, to even out the gel.
3. Let sit for 30 minutes. Excess water was removed before adding the stacking gel.
4. Samples were sonicated at following settings:
    a. Time: 35 sec, pulse: 05, pause: 2, amplitude: 25 %
    b. Sonicator was washed with dH_2O between each sample.
5. Stacking gel was made (Table 9), and 2 mL were added on top of the separating gel. Combs were put in place. Gels were ready in 30 min.
6. A 10 % 2-mercaptoetanol with bromophenyl blue solution was made, and 10 µL of this solution was mixed with 90µL of the samples into new eppendorf tubes with screw cap. Solutions were mixed.
7. The gels were removed from the Mini-Protean Tetra Cell casting frame and placed in a new cell casting frame for protein electrophoresis. SDS-PAGE running buffer was added before 12µL of the samples were applied to each well of the gels, after removing the combs. 2µL loading marker was added to the first well of each gel. The voltage was set to 100V and ampere was noted. Electrophoresis was stopped and ampere set to a constant equal to the noted value for 1-1.5 hours.
8. When the front marker had almost reached the end of the gels, electrophoresis was stopped.

Protein transfer:

9. Transfer buffer with methanol was made (Table 8)

10. A tray was filled with transfer buffer with methanol and 4 x black pads, 4 x Whatman 3 mm filter paper, 2 x nitro cellulose membranes is soaked.
11. Inside gel holder cassette, the pads, filter paper and nitrocellulose membrane was added then the gels were put carefully on top. Then filter paper and a black pad was added on top before closing the cassette. Repeated for all four gels in two cassettes. To avoid air bubbles, a rolling pin was used.
12. The gel holder cassette was placed in the box together with a freezing element and ice. Transfer buffer with methanol was added.
13. Lid was put on, and electricity connected. Voltage was set to 35V. Electrophoresis has started when bubbles appears in the chamber. Run over night.

Ponceau S staining

14. Two trays are needed. One with red Ponceau S stain and one with distilled water.
15. Remove nitrocellulose membranes from cassette, and cut the membranes to fit the trays without cutting the proteins.
16. Membranes are tilted in distilled water before tilting in Ponceau S stain.
17. When protein bonds appear, wash off the excess color with distilled water.
18. Membranes are set to dry in dark place.
19. Mark membranes with infrared pen.

Blocking and protein detection

20. When membranes are dry, they are put in a black box and added 5 mL 5% skim milk solution. Tilt 30 min.

    5% skim milk solution:
    2.5 g skim milk powder
    50 mL TBS-T 1x Tris with Tween

21. Primary antibody is added after 30 min, after mixing the antibody with 5% skim milk solution with TBS-T 1x Tris with Tween (Table 8). Tilted over night in cold storage room.
22. The following day membranes are washed with TBS-T solution 3x5 min on tilting machine.

23. Secondary antibody is added and incubated 1-2 hours at room temperature (Table). Secondary antibody is diluted according to table x and mixed with skim milk solution.

After incubation, membranes are washed with cold TBS-T solution 3x5 min. Membranes are put to dry in dark place before analyzed at Odyssey CLx Infrared Imaging System.

Table 8: *Recipe for reagents used in SDS-PAGE and Western blotting analysis. *denotes work performed in collaboration with laboratory technicians at NIOM.*

Reagent	Total volume	Recipe
10% APS	1 mL	0.1 g APS, dH_2O to final volume
10 % SDS	100 mL	10 g SDS, dH_2O to final volume
Running buffer, pH 8.3 *	1000 mL	3.03 g Tris-base, 14.41 f Glycine, 1 g SDS, dH_2O to final volume, adjust pH
Sample buffer, pH 7 *	100 mL	12 g SDS, 1.817 g Tris-base, 30 g Glycerol, dH_2O to final volume, adjust pH
TBS-T, pH 7.5 *	1000 mL	6.06 g Tris-base, 8.76 g NaCl, 1 mL Tween 20, dH_2O to final volume, adjust pH
Transfer buffer	2000 mL	6.06 g Tris-base, 28.82 g Glycine, 400 mL Methanol, dH_2O to final volume
Tris 0.5 M, pH 6.8 *	100 mL	6.06 g Tris-base, dH_2O to final volume, adjust pH
Tris 1.5 M, pH 8.8 *	100 mL	18.2 g Tris-base, dH_2O to final volume, adjust pH

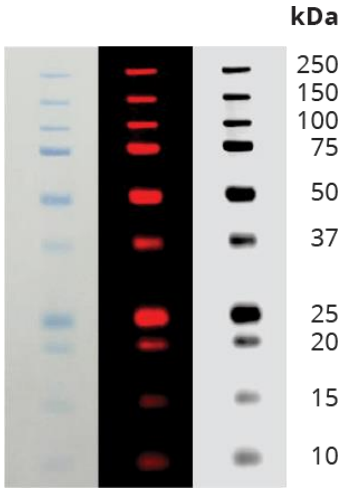

Figure 23: *Odyssey One-Color Protein Molecuar weight Marker used in Western blotting.*

Table 9*: Recipe for 4 x 10 % SDS-PAGE separating gel and stacking gel*

Components	Separating gel	Stacking gel
SDS (10%)	300 µL	100 µL
30% Acrylamide/bis solution 32.5:1	10 mL	1.3 mL
1.5 M Tris (pH 8.8)	7.5 mL	-
0.5 M Tris (pH 6.8)	-	2.5 mL
dH_2O	11.9 mL	6.1 mL
APS (10%)	300 µL	50 µL
TEMED	12 µL	10 µL

Table 10: *Antibodies used in Western blot protocol*

Antibody	Produced in	Product number	Supplier	Molecular weight
Heme oxygenase 1 (HO-1)	Rabbit	P249	Cell Signalling Technologies, USA LiCor	Filter: 800 CW mW: 28 kDA Dilution: 1:5000
Anti-Heme Oxygenase 1 (ab13243)	Rabbit		abcam	Filter: 800 CW mW: 32 Dilution: 1:2000
α-Tubulin				Filter: 700 CW Mw: 50 kDA Dilution:
β-actin				Filter: 700 CW Mw: 42 kDA Dilution:
Goat anti-rabbit	Goat			Filter: 800 CW mW: Dilution: 1:5000
Goat anti-rabbit	Goat			Filter: 700 CW mW: Dilution:

Appendix 9 Supplementary

Table 11: *List of reagents and chemicals*

Chemical compound	CAS	Product number	Supplier
2-Merceptoethanol	60-24-2	M6250	Sigma-Aldrich, St. Louis, USA
2-hydroxyethylmethylacrylate (HEMA)	868-77-9	477028	Sigma-Aldrich, St. Louis, USA
30 % Acrylamide/Bis solution	79-06-1 (acrylamide)110-26-9 (N,N'-methylenediacrylamide)	161-0158	Bio-Rad Laboratories, Inc., CA, USA
5-(and-6)chloromethyl-2',7'-dichlorodihydrofluorescein diacetate, acetyl ester (CM-H2-DCFDA)	-	C6827	ThermoFisher scientific, InvitrogenTM
Ammonium persulfate (APS)	7727-54-0	A3678	Sigma-Aldrich, St. Louis, USA
Antibiotics (penicillin, streptomycin)	15140122		ThermoFisher scientific, GibcoTM
Bromphenol blue sodium salt	62625-28-9	B8026	Sigma-Aldrich, St. Louis, USA
Bovine calf serum	-	-	Sigma-Aldrich, St. Louis, USA
Dihydrorhodamine 123 (DHR)	-	D23806	ThermoFisher scientific, InvitrogenTM
Dimethyl sulphoxide (DMSO)	67-68-5	116743	Merck KGaA, Darmstadt, Germany
Distilled water	-	-	NIOM, Oslo, Norway
DMEM	BE12-709F	7MB075	Lonza, Verviers, Belgium
Fetal Bovine Serum (FBS)	-	F4135	Sigma-Aldrich, St. Louis, USA
Glutamine (L)	-	-	ThermoFisher scientific, GibcoTM
Hoechst 33342	23491-52-3	B2261	Sigma-Aldrich, St. Louis, USA
Horse serum	1671319	-	ThermoFisher scientific, GibcoTM
Liquid nitrogen	-	-	NIOM, Oslo
Loading cursor (Molecular Weight Markers)	64066824	928-40000	LiCor
Methanol	67-56-1	106007	Merck KGaA, Darmstadt, Germany
Millipore water			NIOM, Oslo
N,N,N,N´,N-tetramethyl-ethylendiamine (TEMED)	110-18-9	T9281	Sigma-Aldrich, St. Louis, USA
Na Pyruvate	BE13-115E		Lonza, Verviers, Belgium
Nanoparticles	-	-	Kisker Biotech GmbH & Co, Steinfurt; Germany)
Nerve Growth Factor (NGF)	-	N6009-25UG	Sigma
Phosphate buffered saline 1x (PBS)	-	BE12702F	Lonza, Verviers, Belgium
Ponceau S	6226-79-5	P-3504	Sigma-Aldrich, St. Louis, USA

Propidium iodide solution (PI)	25535-16-4	70335	Sigma-Aldrich, St. Louis, USA
Skim milk powder	-	70166	Sigma-Aldrich, St. Louis, USA
Sodium dodecyl sulfate (SDS)	151-21-3	L4390	Sigma-Aldrich, St. Louis, USA
Sodium dodecyl sulphate (SDS)	151-21-3	L4390	Sigma-Aldrich, St. Louis, USA
Thiazolyl Blue Tetrazolium bromide (MTT solution)	298-93-1	M2128	Sigma-Aldrich, St. Louis, USA
Trypsin	-	-	Sigma-Aldrich, St. Louis, USA
Tween 20	9005-64-5	822184	Merck KGaA, Darmstadt, Germany

Table 12: *List of equipment and software*

Product	**Producer**
Accuri C6 Flow Cytometer	BD Bioscience, Bedford, MA, USA
BD Accuri C6 Software ver. 1.0.264.21	BD Bioscience, Bedford, MA, USA
Cell culture hood, SCANLAF, Mars safety class 2	Labogene, Denmark
Cell scraper	Sigma-Aldrich, St. Louis, USA
Centrifuge, Rotina 35R	Hettic, Germany
CO_2-incubator (SANYO MCO-18AIC(UV))	Suprplus Solutions, LLC, USA
Electric pipette, Pipetboy	INTEGRA Biosciences AG, Switzerland
Electrophoresis systems and blotting module	Bio-Rad Laboratories, Inc., CA, USA
Gen5 1.11	BioTek Instruments, Inc
GraphPad Prism 7 software	GraphPad Software, CA, USA
Mini Trans-Blot cell	Bio-Rad Laboratories, Inc., CA, USA
Mini-PROTEAN Tetra Cell	Bio-Rad Laboratories, Inc., CA, USA
Mini-PROTEAN Tetra handcast systems	Bio-Rad Laboratories, Inc., CA, USA
Nitrile gloves	VWR
Moxi Z, Mini Automated Cell Counter	ORFLO Technologies, ISA
Nitrocellulose blotting membrane 0.2 □m	GE Healthcare
Odyssey CLx Western Blot scanner	LiCor Biosciences, Hamburg, Germany
Olympus BX51-TF Fluorescence Microscope	Olympus, Germany
Olympus C7070 Camera	Olympus, Germany
Olympus D80 Camera	Olympus, Germany
Olympus DP controller, Olympus Optical CO, LTD (2002)	Olympus, Germany
Olympus fluoview FV1200 Confocal Laser Scanning Microscope	Olympus, Germany
Sonics Vibra Cell TM VCX 130	Sonics & Materials Inc., CT, USA
Sterile 12, 24 and 96 sample well-plates, non coated	Costar Cornar Incorporated, USA
Sterile 24 and 96 sample well-plates, coated	Costar Cornar Incorporated, USA
Sterile cell culture flask 75 cm^2	Falcon BD Biosciences, USA
Sterile Cell dishes 20mm, 40mm	Costar Cornar Incorporated, USA
Sterile fine pipette tipps	VWR International GmbH, Darmstadt, Germany
Sterile pipettes	Thermo Scientific, USA
Synergy H1 hybrid reader (plate reader)	BioTek Instruments, Inc.
Up-Cell well-plates (Nunc)	Sigma-Aldrich, St. Louis, USA
Whatman Chromatography paper 3 mm CHR	Whatman

Appendix 10: Supplementary results

MTT-assay

ATCC cells

A-1

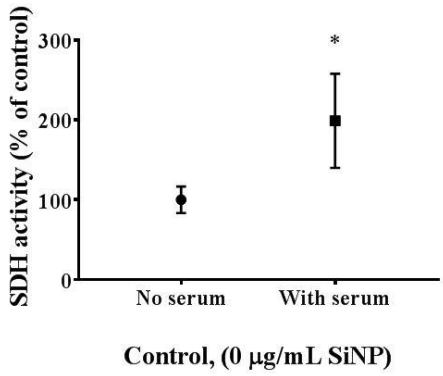

A-2

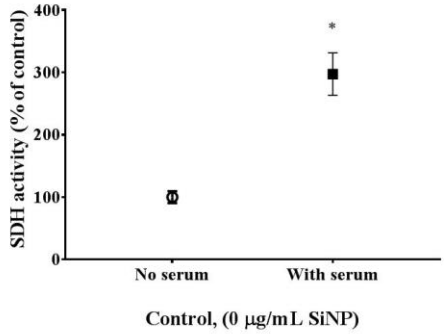

Subclone cells

A-2

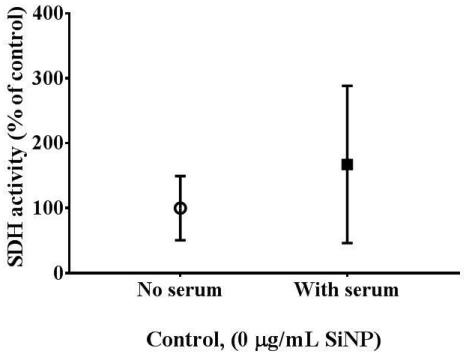

B-2

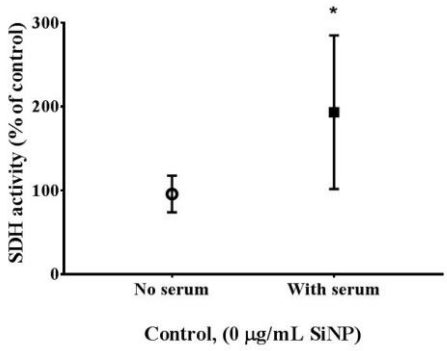

Figure 24: *Measured SDH-activity after 24 (A) and 48 hours (B) of SiNP exposure, normalized to serum free control (0). A-1 and B-1) ATCC cells, A-2 and B-2) subclone cells. All statistical analysis is performed by One-way ANOVA, Dunnett's multiple comparison test and test for linear trend between column mean and left to right column order. The results are shown as mean ± SD (n=3), *denotes significant result ($p \leq 0.05$).*

Oxidative stress

ATCC cells **Subclone cells**

A-1 **A-2**

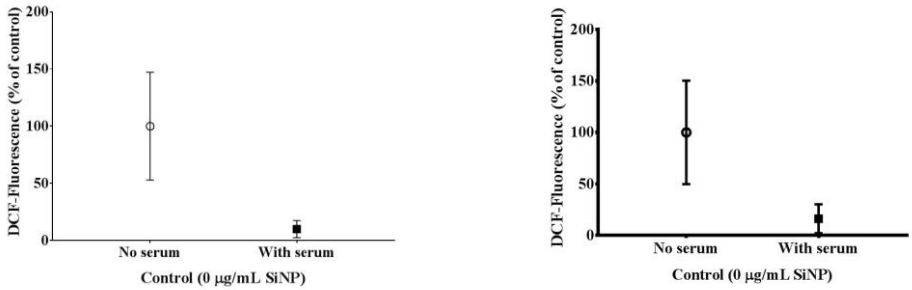

B-1

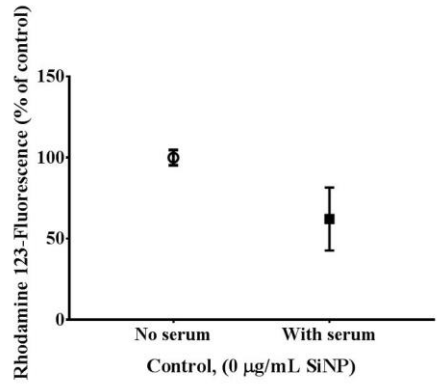

Figure 25: *Controls. Fluorescence measured after 3 h SiNP exposure. Normalized to serum free control. A-1 and B-1) ATCC cells, flow cytometer, A-2) Subclone cells, plate reader. No significant results were found in controls.*

Western blot

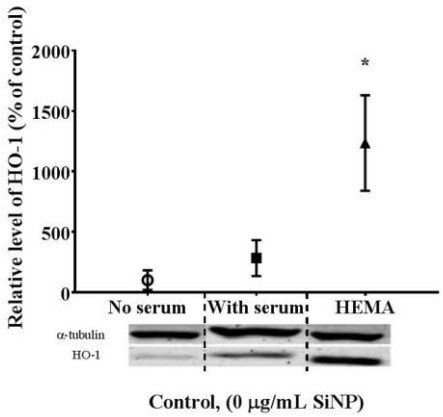

Figure 26: *Relative level of HO-1 after 24 hours of SiNP exposure, normalized to serum free control. The positive control (HEMA) was significantly different from the other controls. All statistical analysis is performed by One-way ANOVA, Dunnett's multiple comparison test and test for linear trend between column mean and left to right column order ($p \leq 0.05$ is considered statistically significant). The results are shown as mean ± SD (n=4). Blots: α-Tubulin (loading control), HO-1 (biomarker enzyme).*